1996

Stability of boundary free shear flows : the effects of diffusion

Louis J. Cumbo
Lehigh University

Cumbo, Louis

Stability of Boundary Free Shear Flows: The Effects of Diffusion

October 13, 1996

STABILITY OF BOUNDARY FREE SHEAR FLOWS: THE EFFECTS OF DIFFUSION

by

Louis J. Cumbo

A Thesis

Presented to the Graduate and Research Committee

of Lehigh University

in the Candidacy for the Degree of

Master of Science

in

Mechanical Engineering

Lehigh University

9-24-96

This thesis is accepted and approved in partial fulfillment of the requirements for the Master of Science.

9/26/96
Date

Thesis Advisor

Chairperson of Department

Acknowledgments

I would like to thank my advisor Dr. Alp Oztekin for his support, instruction and patience in helping me complete this work. I would also like to thank Dr. Antonios Liakopoulos for his additional advice and guidance.

I wish to express my love and appreciation to my parents and sister, who's faith and support were essential in helping me complete my graduate studies. Finally, I would like to recognize my friends here at Lehigh who's assistance and inspiration were essential in completing my graduate work as well as coping with life in general, along with making my experience here memorable and worthwhile.

Table of Contents

Figures

ABSTRACT

Boundary-free shear flow is studied using linear stability theory. The flow is analyzed assuming variable viscosity due to binary diffusion across the shear layer. This leads to the basis and main difficulty of this study, which is a direct coupling of the momentum and species equations used in both the base state calculations as well as the stability analysis.

Linear stability analysis is used to examine the effect of a variable concentration profile on the stability of the flow. It is found that for the flow to be stable for all wave numbers the Reynolds number has to be zero. This is in agreement with constant-viscosity shear flow stability theory. The effect of increasing the dependence of the flow stability on the variable concentration profile (increasing the Schmidt number) is found to be destabilizing.

CHAPTER 1

INTRODUCTION

1.1 Motivation and Previous Work

The problem of predicting stability of free shear flows is of great importance. These types of flows are found in studying natural conditions such as in the atmosphere and the ocean, as well as in engineering situations, such as industrial applications and in aerodynamics. It is vital to understand the mechanisms that control the stability characteristics of free shear flows. This understanding allows for the design of processes that may either passively depend on flow stability or may actively govern the development of the flow.

Boundary-free flows, such as mixing layers, wakes, and jets, are highly unstable when compared to bounded flows. This is attributed to the fact that these flows have an inflection point in the velocity profile, which is associated with inviscid instability. This results in these flows having minute critical Reynolds numbers, the highest Reynolds number for which the flow is stable for all wave numbers of a disturbance, and a larger range of wave numbers for which these flows are unstable when compared to flows that do not have a velocity profile inflection. More specifically, the free shear layer has a critical Reynolds number of zero, or rather, the flow is not stable for all wave numbers for any finite value of Re. This is contrary to the stability behavior of bounded flows, which are completely stable in the inviscid case. For the viscous case it is shown that viscosity has a stabilizing effect.

Due to the apparent stabilizing effect of viscosity on free shear flows, the effects of variable viscosity are worth examining. This investigation, which is the goal of this work, will be discussed in more detail at the end of this chapter.

The initial studies of linear instability of mixing layers in incompressible, parallel, inviscid flows were performed by Helmholtz and Kelvin (Azaiez, 1993). The instability mode they discovered, which is referred to as Kelvin-Helmholtz instability, involves a growing wavy disturbance across the surface located where the initial velocity profile is discontinuous. Rayleigh (Azaiez, 1993) developed his point-of-inflection theorem from the study of incompressible, parallel, inviscid flows with continuous velocity profiles. This theorem proved that a necessary (but not sufficient) condition for instability is that the initial (basic) velocity profile has an inflection point, for inviscid flows. Fjørtoft's (Panton, 1984) theorem improved on Rayleigh's statement by being more selective. It shows that not all profiles with an inflection point have the necessary condition for instability. It was shown by Tollmien (Azaiez, 1993) that an inflection point is not only necessary but also a sufficient condition for instability, as well.

The study of instability of viscous flows was aided by the equation developed by Orr and Sommerfeld (Panton, 1984) and named the Orr-Sommerfeld equation. In the past it was very difficult to solve. For the Blasius profile of a boundary layer flow it was over twenty years until the first successful solutions by Tollmien and Schlicting (Panton, 1984) were developed for the Orr-Sommerfeld equation. It should also be noted that these original solutions were only approximations.

Squire (Panton,1984) showed that for incompressible viscous flows, a two-dimensional disturbance is more unstable than a three-dimensional disturbance. This led the way for future researchers to use a less complex two-dimensional disturbance when seeking the stability boundary for a certain flow type. The first stability investigation of a realistic free boundary-layer type of flow was done by Lesson (1950). However, his power-series-expansion method of solving the stability equations allowed for only studying flows with large Reynolds numbers, therefore he did not report a Reynolds number for which the flow was completely stable. Esch (1957) reported that a boundary free flow has a critical Reynolds number of zero; however, he studied a piece-wise linear flow. Tatsumi and Gotoh (1959) studied the stability problem of boundary free flows with a general form of the velocity profile. They discovered that the critical Reynolds numbers for these flows was identically zero.

For small wave-numbers of the disturbance, Drazin and Howard (1962) calculated the instability characteristics of the hyperbolic-tangent profile. Michalke (1964 and 1965) obtained the eigenvalues and eigenfunctions of the inviscid Rayleigh equation for this same profile. Betchov and Szewczyk (1963) examined the stability of a Newtonian viscous flow with the hyperbolic-tangent profile by solving the Orr-Sommerfeld equation. They found that the flow was not stable for all wave numbers for any value of Reynolds number, which implied that the critical Reynolds number was zero. Perhaps, due to the conclusion that there is not a finite Reynolds number for boundary-free shear flows, or that the parallel flow assumption is not completely satisfactory when investigating flows with low Reynolds numbers, there is not much

further investigation into the linear stability of boundary-free flows. Rather, more recent studies investigate the transition to turbulence of these flows which assume large Reynolds numbers or mechanisms that involve non-linear stability. Such as the work done by Azaiez and Homsy (1993), where they investigated the linear stability of viscoelastic fluids. Also, Metcalfe *et al.* (1987) examined the effects of the interaction between linear and non-linear flow states on stability in the transition to turbulence regime.

1.2 Goals of the Present Work

The question remains whether the effect of viscosity variation in the flow would stabilize it enough so that it would have a finite critical Reynolds number, or if it will still remain that the critical *Re* is zero. Even less explored is a boundary-free shear flow with a concentration gradient present. This would result in the combination of the transport of species with the original momentum transport phenomenon. In addition, the viscosity of the fluid would be a function of the level of concentration. This would lead to direct coupling of these two occurrences.

Due to the lack of studies done, to the authors' knowledge, in boundary free shear flows with a concentration gradient, we investigate the linear stability of these flows. We assume that viscosity varies with concentration. Both the momentum (velocity) layer and concentration (mixing) layer equations will be considered in the analysis. Due to the relation of viscosity to concentration both equations are strongly coupled and the effect of both layers on the stability of the flow will be examined. It is the intention of this work to determine the importance of including the concentration

layer in addition to the velocity profile in predicting the onset of instability in boundary-free shear flows.

In Chapter 2, we develop the governing equations for the basic state. Using boundary layer assumptions we present a similarity solution for the steady flow field. Next, we derive the equations used in the linear stability analysis, using the parallel flow assumption.

In Chapter 3, the numerical techniques used to solve the basic state equations and the eigenvalue problem for the stability equations are described in detail.

In Chapter 4, we first determine the validity of the computer code used to perform the stability analysis. Next we examine the results of the basic state profiles, and the effects of varying the various momentum and diffusion parameters on these respective profiles. Finally, we investigate the stability of the basic flow field for various parameters.

In Chapter 5, explanations for the major results are presented, as well as possible suggestions for the effects of viscosity variations and the diffusion layer on the stability of boundary-free shear flows.

CHAPTER 2

FORMULATION

2.1 Governing Equations

In deriving the governing equations for the momentum transport and diffusion in the shear layer shown in figure 1, we begin with the two-dimensional continuity, momentum and species equations, assuming constant density, and a Newtonian fluid

$$\nabla_1 \cdot \tilde{\mathbf{u}}_1 = 0, \tag{2.1a}$$

$$-\nabla_1 \tilde{\mathbf{p}}_1 + \nabla_1 \cdot (\mu_1 \dot{\gamma}_1) = \rho_1 (\tilde{\mathbf{u}}_1 \cdot \nabla_1)\tilde{\mathbf{u}}_1 + \rho_1 \frac{\partial \tilde{\mathbf{u}}_1}{\partial t}, \tag{2.1b}$$

$$\frac{\partial \tilde{c}_1}{\partial t} + \tilde{\mathbf{u}}_1 \cdot \nabla_1 \tilde{c}_1 = \nabla_1 \cdot (D_1 \nabla \tilde{c}_1), \tag{2.1c}$$

$$\nabla_2 \cdot \tilde{\mathbf{u}}_2 = 0, \tag{2.1d}$$

$$-\nabla_2 \tilde{\mathbf{p}}_2 + \nabla_2 \cdot (\mu_2 \dot{\gamma}_2) = \rho_2 (\tilde{\mathbf{u}}_2 \cdot \nabla_2)\tilde{\mathbf{u}}_2 + \rho_2 \frac{\partial \tilde{\mathbf{u}}_2}{\partial t}, \tag{2.1e}$$

$$\frac{\partial \tilde{c}_2}{\partial t} + \tilde{\mathbf{u}}_2 \cdot \nabla_2 \tilde{c}_2 = \nabla_2 \cdot (D_2 \nabla_2 \tilde{c}_2), \tag{2.1f}$$

Here, subscript 1 corresponds to $y > 0$, and 2 to $y < 0$. Also, $\tilde{\mathbf{u}}$ represents the two-dimensional velocity vector, $\tilde{\mathbf{p}}$ is pressure, μ is absolute viscosity, $\dot{\gamma}$ is the rate-of-strain tensor, ρ is density, D is the binary mass diffusion coefficient for the two fluids, and $\tilde{c}$ is the concentration.

The boundary conditions far from the mixing layer of the two fluids, as $y \to +\infty$ and $y \to -\infty$, are

$$y \to +\infty \qquad \tilde{u}_1 \to U_1 \qquad \tilde{c}_1 \to C_1$$

$$y \to -\infty \qquad \tilde{u}_2 \to U_2 \qquad \tilde{c}_2 \to C_2$$

where U_1, U_2, C_1, and C_2 are the flow velocities and concentrations for the two initially separated fluid layers. Here, $\tilde{u}_1$, $\tilde{u}_2$, $\tilde{c}_1$ and $\tilde{c}_2$ represent the local dimensional flow velocities and concentrations.

2.2 Boundary Layer Analysis

It is assumed that the boundary layer thickness of both the momentum layer as well as the diffusion layer is relatively small. Therefore, the following inequalities are applied:

$$u >> \mathrm{v}$$

$$\frac{\partial u}{\partial y} >> \frac{\partial u}{\partial x}, \frac{\partial \mathrm{v}}{\partial y}, \frac{\partial \mathrm{v}}{\partial x} \qquad \text{Velocity boundary layer}$$

$$\frac{\partial c}{\partial y} >> \frac{\partial c}{\partial x} \qquad \text{Concentration boundary layer.}$$

These assumptions imply that the velocity component in the x-direction is much greater than in the y-direction, and gradients normal to the x-direction are much larger than those parallel to it. Also, species diffusion rates are assumed to be much larger in the y-direction relative to the diffusion rates in the direction of the mean flow. This yields the following steady dimensional equations (Incropera & DeWitt, 1990):

$$\frac{\partial \tilde{u}_1}{\partial \tilde{x}_1} + \frac{\partial \tilde{\mathrm{v}}_1}{\partial \tilde{y}_1} = 0 \tag{2.2a}$$

$$\tilde{u}_1 \frac{\partial \tilde{u}_1}{\partial \tilde{x}_1} + \tilde{\mathrm{v}}_1 \frac{\partial \tilde{u}_1}{\partial \tilde{y}_1} = \frac{\partial}{\partial \tilde{y}_1}\left(\tilde{\nu}_1 \frac{\partial \tilde{u}_1}{\partial \tilde{y}_1}\right) \tag{2.2b}$$

$$\tilde{u}_1 \frac{\partial \tilde{c}_1}{\partial \tilde{x}_1} + \tilde{v}_1 \frac{\partial \tilde{c}_1}{\partial \tilde{y}_1} = D \frac{\partial^2 \tilde{c}_1}{\partial \tilde{y}_1^2} \tag{2.2c}$$

$$\frac{\partial \tilde{u}_2}{\partial \tilde{x}_2} + \frac{\partial \tilde{v}_2}{\partial \tilde{y}_2} = 0 \tag{2.2d}$$

$$\tilde{u}_2 \frac{\partial \tilde{u}_2}{\partial \tilde{x}_2} + \tilde{v}_2 \frac{\partial \tilde{u}_2}{\partial \tilde{y}_2} = \frac{\partial}{\partial \tilde{y}_2}\left(\tilde{\nu}_2 \frac{\partial \tilde{u}_2}{\partial \tilde{y}_2} \right) \tag{2.2e}$$

$$\tilde{u}_2 \frac{\partial \tilde{c}_2}{\partial \tilde{x}_2} + \tilde{v}_2 \frac{\partial \tilde{c}_2}{\partial \tilde{y}_2} = D \frac{\partial^2 \tilde{c}_2}{\partial \tilde{y}_2^2} \tag{2.2f}$$

The simplified equations are then non-dimensionalized by scaling length, velocity, viscosity, and concentration with (H, U_1, ν_0, C_1) respectively. Here $H = \delta$ is the characteristic length, δ is the shear layer thickness, and ν_o denotes the reference kinematic viscosity. This yields the following dimensionless governing equations,

$$\frac{\partial u_1}{\partial x_1} + \frac{\partial v_1}{\partial y_1} = 0, \tag{2.3a}$$

$$u_1 \frac{\partial u_1}{\partial x_1} + v_1 \frac{\partial u_1}{\partial y_1} = \frac{1}{Re} \frac{\partial}{\partial y_1} (\nu_1 \frac{\partial u_1}{\partial y_1}), \tag{2.3b}$$

$$u_1 \frac{\partial c_1}{\partial x_1} + v_1 \frac{\partial c_1}{\partial y_1} = \frac{1}{Re\, Sc} \frac{\partial^2 c_1}{\partial y_1^2}, \tag{2.3c}$$

$$\frac{\partial u_2}{\partial x_2} + \frac{\partial v_2}{\partial y_2} = 0, \tag{2.3d}$$

$$u_2 \frac{\partial u_2}{\partial x_2} + v_2 \frac{\partial u_2}{\partial y_2} = \frac{1}{Re} \frac{\partial}{\partial y_2} (\nu_2 \frac{\partial u_2}{\partial y_2}), \tag{2.3e}$$

$$u_2 \frac{\partial c_2}{\partial x_2} + v_2 \frac{\partial c_2}{\partial y_2} = \frac{1}{Re\, Sc} \frac{\partial^2 c_2}{\partial y_2^2}. \tag{2.3f}$$

The dimensionless parameter *Re* represents the global Reynolds number $(U_1\delta/\nu_o)$, and *Sc* represents the Schmidt number (ν_o/D).

2.3 Basic State Similarity Solution

To solve the system of governing equations we use the similarity solution developed by Blasius. For simplicity, the subscripts denoting either region one or two are omitted for development of the similarity variable. First, we define the velocity components in terms of a stream function $\psi(x,y)$ by using equations 2.3a and 2.3d

$$u \equiv \frac{\partial \psi}{\partial y} \quad \text{and} \quad v \equiv -\frac{\partial \psi}{\partial x} \tag{2.4}$$

The continuity equations (2.3a and 2.3d) are now satisfied and no longer needed. We now define a similarity parameter $\eta(x,y)$ such that $\eta = y/\delta$. It is assumed that δ is a function of ν_o, U_1, and x such that

$$\delta = g\left(\frac{U_1\tilde{x}}{\nu_o}\right) \Rightarrow \delta \propto \sqrt{\frac{\nu_o\tilde{x}}{U_1}}$$

where $\tilde{x}$ is a dimensional variable and g represents an arbitrary function. Now, η is defined by

$$\eta \equiv \frac{\tilde{y}}{\delta} = \frac{\tilde{y}}{\sqrt{\tilde{x}\frac{\nu_o}{U_1}}}. \tag{2.5}$$

Recalling that H is defined by δ, and non-dimensionalizing the equation for η yields the following expression,

$$\eta \equiv y\sqrt{\frac{Re}{x}}. \tag{2.6}$$

The stream function can now be written in terms of η. Recalling that $u = \frac{\partial \psi}{\partial y}$ we can write an integral equation for ψ,

$$\psi = \int_{-y}^{y} u\, dy. \tag{2.7}$$

Note that the velocity component u is some function of η, where $u = F(\eta)$.

Also, we have the following relations,

$$dy = \sqrt{\frac{x}{Re}}\, d\eta, \tag{2.8}$$

$$\psi = \int_{-\eta}^{\eta} \sqrt{\frac{x}{Re}} F(\eta)\, d\eta. \tag{2.9}$$

Introducing a function $f(\eta)$ such that,

$$f(\eta) = \int_{-\eta}^{\eta} F(\eta)\, d\eta,$$

ψ can be written as $\psi = f(\eta)\sqrt{\frac{x}{Re}}$, and the velocity terms are written in terms η using the chain rule,

$$u = \frac{\partial f}{\partial \eta}, \tag{2.10}$$

$$v = \frac{1}{2\sqrt{Re\, x}}\left(\eta f' - f\right). \tag{2.11}$$

Substituting these terms into the momentum and species equations (2.3b, 2.3c, 2.3e, and 2.3f) we get the following nonlinear, differential equations for f_1, f_2, c_1, and c_2,

$$\frac{\partial^3 f_1}{\partial \eta^3}+\frac{1}{\nu}\frac{\partial^2 f_1}{\partial \eta^2}\left(\frac{f_1}{2}+\frac{\partial \nu}{\partial \eta}\right)=0 \tag{2.12}$$

$$\frac{\partial^2 c_1}{\partial \eta^2}+\frac{Sc}{2} f_1 \frac{\partial c_1}{\partial \eta}=0 \tag{2.13}$$

$$\frac{\partial^3 f_2}{\partial \eta^3}+\frac{1}{\nu}\frac{\partial^2 f_2}{\partial \eta^2}\left(\frac{f_2}{2}+\frac{\partial \nu}{\partial \eta}\right)=0 \tag{2.14}$$

$$\frac{\partial^2 c_2}{\partial \eta^2}+\frac{Sc}{2} f_2 \frac{\partial c_2}{\partial \eta}=0 \tag{2.15}$$

In terms of η the boundary conditions are written as:

$$\eta \to +\infty \qquad \frac{\partial f_1}{\partial \eta} \to 1 \qquad c_1 \to 1 \tag{2.16}$$

$$\eta \to -\infty \qquad \frac{\partial f_2}{\partial \eta} \to U^* \qquad c_2 \to C^* \tag{2.17}$$

where $U^* = U_2 / U_1$ and $C^* = C_2 / C_1$.

At the location where the initial mixing occurs y = 0. Since the motion is steady at the interface the stream function is equal to zero. This leads to the following additional boundary conditions,

$$\eta = 0, \qquad f_1 = f_2 = 0. \tag{2.18}$$

The velocity should be continuous at this location. Therefore, the condition must exist such that for

$$\eta = 0, \qquad f_1' = f_2', \tag{2.19}$$

which ensures that u and v will both be continuous.

Also, the tangential stress should be continuous. For the boundary layer, using the previous assumptions in Chapter 2, the tangential stress can be approximated as $\mu(\partial u / \partial y)$. This leads to the following condition,

$$f_1'' = f_2'' \quad \text{at } \eta = 0. \tag{2.20}$$

Likewise, the concentration, as well as the rate of change in the concentration profile, at this location should be continuous. Therefore, the following conditions exist:

$$\text{at } \eta = 0, \qquad c_1 = c_2, \tag{2.21}$$

$$\text{at } \eta = 0, \qquad c_1' = c_2'. \tag{2.22}$$

2.4 Linear Disturbance Equations

To analyze the stability of the shear flow, we first begin with the dimensional governing equations for an incompressible Newtonian fluid,

$$\frac{\partial \tilde{u}_k}{\partial \tilde{x}_k} + \frac{\partial \tilde{v}_k}{\partial \tilde{y}_k} = 0, \tag{2.23a}$$

$$\frac{\partial \tilde{u}_k}{\partial \tilde{t}} + \tilde{u}_k \frac{\partial \tilde{u}_k}{\partial \tilde{x}} + \tilde{v}_k \frac{\partial \tilde{u}_k}{\partial \tilde{y}} = -\frac{1}{\rho}\frac{\partial \tilde{p}_k}{\partial \tilde{x}} + \frac{\partial}{\partial \tilde{x}}\left(2\tilde{\nu}_k \frac{\partial \tilde{u}_k}{\partial \tilde{x}}\right) + \frac{\partial}{\partial \tilde{y}}\left(\tilde{\nu}_k\left[\frac{\partial \tilde{u}_k}{\partial \tilde{y}} + \frac{\partial \tilde{v}_k}{\partial \tilde{x}}\right]\right), \tag{2.23b}$$

$$\frac{\partial \tilde{v}_k}{\partial \tilde{t}} + \tilde{u}_k \frac{\partial \tilde{v}_k}{\partial \tilde{x}} + \tilde{v}_k \frac{\partial \tilde{v}_k}{\partial \tilde{y}} = -\frac{1}{\rho}\frac{\partial \tilde{p}_k}{\partial \tilde{y}} + \frac{\partial}{\partial \tilde{y}}\left(2\tilde{\nu}_k \frac{\partial \tilde{v}_k}{\partial \tilde{x}}\right) + \frac{\partial}{\partial \tilde{x}}\left(\tilde{\nu}_k\left[\frac{\partial \tilde{u}_k}{\partial \tilde{y}} + \frac{\partial \tilde{v}_k}{\partial \tilde{x}}\right]\right), \tag{2.23c}$$

$$\frac{\partial \tilde{c}_k}{\partial \tilde{t}} + \tilde{u}_k \frac{\partial \tilde{c}_k}{\partial \tilde{x}} + \tilde{v}_k \frac{\partial \tilde{c}_k}{\partial \tilde{y}} = \frac{\partial}{\partial \tilde{x}}\left(D\frac{\partial \tilde{c}_k}{\partial \tilde{x}}\right) + \frac{\partial}{\partial \tilde{y}}\left(D\frac{\partial \tilde{c}_k}{\partial \tilde{y}}\right). \tag{2.23d}$$

Where k = 1, 2 with no summation over k. These equations are then normalized by scaling length, velocity, viscosity, concentration, pressure and time with

$(H, U_1, \nu_0, C_1, \rho U_1^2, H/U_1)$ respectively. Also, it is assumed that the density is equal in both regions 1 and 2. This yields the following dimensionless equations:

$$\frac{\partial u_k}{\partial x} + \frac{\partial v_k}{\partial y} = 0, \tag{2.24a}$$

$$\frac{\partial u_k}{\partial t} + u_k \frac{\partial u_k}{\partial x} + v_k \frac{\partial u_k}{\partial y} = -\frac{\partial p_k}{\partial x} + \frac{2}{Re}\frac{\partial}{\partial x}\left(\nu_k \frac{\partial u_k}{\partial x}\right) + \frac{1}{Re}\frac{\partial}{\partial y}\left(\nu_k\left[\frac{\partial u_k}{\partial y} + \frac{\partial v_k}{\partial x}\right]\right), \tag{2.24b}$$

$$\frac{\partial v_k}{\partial t} + u_k \frac{\partial v_k}{\partial x} + v_k \frac{\partial v_k}{\partial y} = -\frac{\partial p_k}{\partial y} + \frac{2}{Re}\frac{\partial}{\partial y}\left(\nu_k \frac{\partial v_k}{\partial x}\right) + \frac{1}{Re}\frac{\partial}{\partial x}\left(\nu_k\left[\frac{\partial u_k}{\partial y} + \frac{\partial v_k}{\partial x}\right]\right), \tag{2.24c}$$

$$\frac{\partial c_k}{\partial t} + u_k \frac{\partial c_k}{\partial x} + v_k \frac{\partial c_k}{\partial y} = \frac{1}{Re\,Sc}\left[\frac{\partial^2 c_k}{\partial x^2} + \frac{\partial^2 c_k}{\partial y^2}\right]. \tag{2.24d}$$

Using the continuity equation (2.24a) we can re-write the momentum equations in the following form,

$$\begin{aligned}\frac{\partial u_k}{\partial t} + u_k \frac{\partial u_k}{\partial x} + v_k \frac{\partial u_k}{\partial y} = -\frac{\partial p_k}{\partial x} + \frac{1}{Re}\Big[&\frac{\partial \nu_k}{\partial x}\frac{\partial u_k}{\partial x} + \nu_k \frac{\partial^2 u_k}{\partial x^2} + \frac{\partial \nu_k}{\partial y}\frac{\partial u_k}{\partial y} \\ &+ \nu_k \frac{\partial^2 u_k}{\partial x^2} + \frac{\partial \nu_k}{\partial y}\frac{\partial v_k}{\partial x} + \frac{\partial \nu_k}{\partial x}\frac{\partial v_k}{\partial y}\Big],\end{aligned} \tag{2.25a}$$

$$\begin{aligned}\frac{\partial v_k}{\partial t} + u_k \frac{\partial v_k}{\partial x} + v_k \frac{\partial v_k}{\partial y} = -\frac{\partial p_k}{\partial y} + \frac{1}{Re}\Big[&\frac{\partial \nu_k}{\partial x}\frac{\partial v_k}{\partial x} + \nu_k \frac{\partial^2 v_k}{\partial x^2} + \frac{\partial \nu_k}{\partial y}\frac{\partial u_k}{\partial y} \\ &+ \nu_k \frac{\partial^2 v_k}{\partial y^2} + \frac{\partial \nu_k}{\partial y}\frac{\partial u_k}{\partial x} + \frac{\partial \nu_k}{\partial x}\frac{\partial u_k}{\partial y}\Big].\end{aligned} \tag{2.25b}$$

To determine the conditions under which a disturbance grows, we assume a quasi-one dimensional flow situation, where the disturbances will be analyzed at a fixed x location. Due to the fact that the base state velocity in the x direction (u) and the concentration (c) are dependent on the function f, which is a function of the similarity variable η, and x is fixed, the base state for these variables depends only on y for the

disturbance equations in this case. For simplification, we assume a parallel flow, or in other words, that the base state velocity in the y direction, v, is zero. We also assume two-dimensional disturbances that vary with time for the x and y velocity components as well as the concentration. This gives the following representations for the velocities, concentration and viscosity:

$$u_k(x,y,t) = \bar{u}_k(y) + \dot{u}_k(x,y,t), \tag{2.26a}$$

$$\mathrm{v}_k(x,y,t) = \dot{\mathrm{v}}_k(x,y,t), \tag{2.26b}$$

$$c_k(x,y,t) = \bar{c}_k(y) + \dot{c}_k(x,y,t), \tag{2.26c}$$

$$\nu_k = \nu_k(c). \tag{2.26d}$$

Substitution of the above into the momentum and species equations, subtracting the base flow, and linearizing disturbance terms yields the following disturbance equations.

$$\frac{\partial \dot{u}_k}{\partial x} + \frac{\partial \dot{\mathrm{v}}_k}{\partial \mathrm{y}} = 0 \tag{2.27a}$$

$$\begin{aligned}\frac{\partial \dot{u}_k}{\partial t} + \bar{u}_k \frac{\partial \dot{u}_k}{\partial x} + \dot{\mathrm{v}}_k \frac{\partial \bar{u}_k}{\partial y} = -\frac{\partial \dot{p}_k}{\partial x} + \frac{1}{Re}\Big[\bar{\nu}_k \frac{\partial^2 \dot{u}_k}{\partial x^2} + \frac{\partial \bar{\nu}_k}{\partial y}\frac{\partial \dot{u}_k}{\partial y} + \frac{\partial \dot{\mathrm{v}}_k}{\partial y}\frac{\partial \bar{u}_k}{\partial y} \\ + \dot{\mathrm{v}}_k \frac{\partial^2 \bar{u}_k}{\partial y^2} + \bar{\nu}_k \frac{\partial^2 \dot{u}_k}{\partial y^2} + \frac{\partial \bar{\nu}_k}{\partial y}\frac{\partial \dot{\mathrm{v}}_k}{\partial x}\Big]\end{aligned} \tag{2.27b}$$

$$\begin{aligned}\frac{\partial \dot{\mathrm{v}}_k}{\partial t} + \bar{u}_k \frac{\partial \dot{\mathrm{v}}_k}{\partial x} = -\frac{\partial \dot{p}_k}{\partial y} + \frac{1}{Re}\Big[\frac{\partial \bar{\nu}_k}{\partial y}\frac{\partial \dot{\mathrm{v}}_k}{\partial y} + \bar{\nu}_k \frac{\partial^2 \dot{\mathrm{v}}_k}{\partial y^2} + \bar{\nu}_k \frac{\partial^2 \dot{\mathrm{v}}_k}{\partial x^2} + \frac{\partial \dot{\mathrm{v}}_k}{\partial x}\frac{\partial \bar{u}_k}{\partial y} \\ - \frac{\partial \bar{\nu}_k}{\partial y}\frac{\partial \dot{u}_k}{\partial x}\Big]\end{aligned} \tag{2.27c}$$

$$\frac{\partial \dot{c}_k}{\partial t} + \bar{u}_k \frac{\partial \dot{c}_k}{\partial x} + \dot{\mathrm{v}}_k \frac{\partial \bar{c}_k}{\partial y} = \frac{1}{Re\,Sc}\left[\frac{\partial^2 \dot{c}_k}{\partial x^2} + \frac{\partial^2 \dot{c}_k}{\partial y^2}\right] \tag{2.27d}$$

Using the disturbance continuity equation (2.24a) we can introduce a disturbance stream function, $\dot{\psi}$, such that

$$\dot{u}_k = \frac{\partial \dot{\psi}_k}{\partial y}, \tag{2.28a}$$

$$\dot{v}_k = -\frac{\partial \dot{\psi}_k}{\partial x}, \tag{2.28b}$$

where

$$\dot{\psi}_k(x,y,t) = \phi_k(y)\, e^{(i\alpha x+\beta t)}. \tag{2.29}$$

In equation (2.29) α is a real positive quantity and $\lambda = 2\,\pi/\alpha$ is the wavelength of the disturbance. The quantity β is a complex parameter such that

$$\beta = \beta_r + i\beta_i$$

where β_i is the circular frequency of the oscillation, and β_r determines the degree of the amplification or damping. The disturbances are damped if $\beta_r < 0$, yet if $\beta_r > 0$, the flow destabilizes with time. The amplitude function, ϕ, of the fluctuation is assumed to depend only on y. From the equation for ψ' we obtain the disturbance components of the velocity:

$$\dot{u}_k(x,y,t) = \phi_k'(y)\, e^{(i\alpha x+\beta t)}, \tag{2.30a}$$

$$\dot{v}_k(x,y,t) = -i\alpha\phi_k(y)\, e^{(i\alpha x+\beta t)}. \tag{2.30b}$$

The primes denote derivatives with respect to y. Likewise, the pressure and concentration disturbances have similar forms with the amplitudes of disturbance being denoted by κ_k, and P_k respectively,

$$\dot{c}_k(x,y,t) = \kappa_k(y)\, e^{(i\alpha x+\beta t)}, \tag{2.30c}$$

$$\dot{p}_k(x,y,t) = P_k(y)\, e^{(i\alpha x+\beta t)}. \tag{2.30d}$$

Substituting equations 2.30a-d into equations 2.27b-d and eliminating pressure we obtain the following disturbance differential equations:

$$\begin{aligned}
&\alpha Re\left[(\bar{u}_k - \frac{i\beta}{\alpha})(i\alpha^2\phi_k - i\phi_k'') + i\bar{u}_k''\phi_k\right] + \bar{v}_k(\phi_k^{iv} - 2\alpha^2\phi_k'' + \alpha^4\phi_k) + \\
&2\frac{d\bar{v}_k}{dc_k}\bar{c}_k'(\phi_k''' - \alpha^2\phi_k') + \left(\frac{d\bar{v}_k}{dc_k}\bar{c}_k'' + \frac{d^2\bar{v}_k}{dc_k^2}\bar{c}_k'^2\right)(\phi_k'' + \alpha^2\phi_k) + \\
&\kappa_k\left(2\bar{u}_k''\frac{d^2\bar{v}_k}{dc_k^2}\bar{c}' + \bar{u}_k'\frac{d^2\bar{v}_k}{dc_k^2}\bar{c}_k'' + \alpha^2\bar{u}_k'\frac{d\bar{v}_k}{dc_k} + \bar{u}_k''\frac{d\bar{v}_k}{dc_k}\right) + \\
&\kappa_k'\left(2\bar{u}_k''\frac{d\bar{v}_k}{dc_k} + 2\bar{u}_k'\frac{d^2\bar{v}_k}{dc_k^2}\bar{c}'\right) + \kappa_k''\bar{u}_k'\frac{d\bar{v}_k}{dc_k} = 0,
\end{aligned} \tag{2.31a}$$

$$\beta\kappa_k + \bar{u}_k i\alpha\kappa_k - i\alpha\phi_k\bar{c}_k' + \frac{1}{Re\,Sc}\left[\alpha^2\kappa_k - \kappa_k''\right] = 0. \tag{2.31b}$$

2.5 Viscosity Dependence

In both the base state and stability equations, the relation of viscosity with concentration is represented by

$$\nu_k = 1 + ac_k^2, \tag{2.32}$$

where a is a positive number. This relation is derived from Swindells et al. (1959), where it is stated that ν_{sp}/c versus c has a positive linear slope, and $\nu_{sp} \equiv \nu/\nu_o - 1$. Assuming constant density and non-dimensionalizing we obtain the relation for viscosity in Eq. (2.32).

CHAPTER 3

NUMERICAL SOLUTION

3.1 Base State Equation

To discretize the problem in a general form, we truncate each sub-domain as,

$$\eta \to \infty, \qquad \eta = b, \tag{3.1a}$$

$$\eta \to -\infty, \qquad \eta = c, \tag{3.1b}$$

and at $\eta = 0$,

$$\eta = 0, \qquad \eta = a. \tag{3.1c}$$

The effect of truncation of the domain will be examined in Chapter 4.

Since we use Chebyshev polynomials we scale the similarity parameter by $z_1 = m_1\eta_1 + n_1$ and $z_2 = m_2\eta_2 + n_2$ for the region that lies between a and b, and a and c respectively, so that each region lies between -1 and +1. The coefficients of the transformation are:

$$m_1 = \frac{2}{b-a} \tag{3.2a}$$

$$n_1 = -1 - \frac{2a}{b-a} \tag{3.2b}$$

$$m_2 = \frac{2}{c-a} \tag{3.2c}$$

$$n_2 = -1 - \frac{2a}{c-a} \tag{3.2d}$$

This leads to the following equations governing the basic flow,

$$f_1''' + \frac{1}{m_1 v_1} f_1'' \left(\frac{f_1}{2Sc} + v_1' \right) = 0, \tag{3.3a}$$

$$c_1'' + \frac{f_1}{2m_1} c_1' = 0, \tag{3.3b}$$

$$f_2'''' + \frac{1}{m_2 \nu_2} f_2''' \left(\frac{f_2}{2Sc} + \nu_2' \right) = 0, \tag{3.3c}$$

$$c_2'' + \frac{f_2}{2m_2} c_2' = 0. \tag{3.3d}$$

where, primes now denote differentiation with respect to z_1 and z_2. The boundary conditions for this system of equations are:

$$f_1(-1) = 0, \tag{3.4a}$$

$$f_2(-1) = 0, \tag{3.4b}$$

$$f_1'(1) = 1, \tag{3.4c}$$

$$f_2'(1) = U^*, \tag{3.4d}$$

$$\frac{m_1}{m_2} f_1'(-1) = f_2'(-1), \tag{3.4e}$$

$$\left(\frac{m_1}{m_2} \right)^2 f_1''(-1) = f_2''(-1), \tag{3.4f}$$

$$c_1(1) = 1, \tag{3.4g}$$

$$c_2(1) = C^*, \tag{3.4h}$$

$$c_1(-1) = c_2(-1), \tag{3.4i}$$

$$c_1(-1) = c_2(-1), \tag{3.4j}$$

$$\left(\frac{m_1}{m_2} \right) c_1'(-1) = c_2'(-1). \tag{3.4k}$$

The resulting system is reduced to a set of nonlinear algebraic equations using a spectral Galerkin Chebyshev approach developed by Zebib (1987). The details are given in Appendix A. Standard Newton iteration is used to reduce these equations to a set of linear equations,

$$\mathbf{Ax} + \mathbf{b} = 0$$

which is solved using the IMSL sub-routine DSLRG.

3.2 Eigenvalue Problem

Our objective is to find conditions for which infinitesimally small disturbance grow for a finite number of critical wavenumbers, and decay for all other wavenumbers. This is the condition for which the flow is unstable, where the real part of β is greater than zero as discussed in the previous chapter.

In Chapter 2, we formulated an eigenvalue problem for two systems of ordinary differential equations on two semi-infinite intervals, coupled by boundary conditions at the interface of these intervals. For convenience we solve the problem on a finite computational domain (c, b). The far field boundary conditions at $y=\pm\infty$, due to the assumption all disturbances in the velocity field as well as in the concentration profile approach zero, are as follows,

$$\text{at } y = b\text{:}\quad u' = v' = c' = 0\text{:}\quad \phi_1 = 0,\quad \phi_1' = 0,\quad \kappa_1 = 0 \tag{3.10a}$$

$$\text{at } y = c\text{:}\quad u' = v' = c' = 0\text{:}\quad \phi_2 = 0,\quad \phi_2' = 0,\quad \kappa_2 = 0. \tag{3.10b}$$

Also, at the interface of these two layers the amplitudes of the disturbances are assumed to be continuous:

$$\text{at } y=a\text{:}\quad \phi_1=\phi_2,\quad \phi_1'=\phi_2',\quad \phi_1''=\phi_2'',\quad \phi_1'''=\phi_2''',\quad \kappa_1=\kappa_2,\quad \kappa_1'=\kappa_2' \tag{3.10c}$$

For all analysis in this study we have used symmetric intervals so that b = -c, where this interval will be referred to as (-L, L). Since we use Chebyshev polynomials in this solution, as in the base solution, we scale the coordinates by $z_1 = m_1 y_1 + n_1$ and $z_2 = m_2 y_2 + n_2$, where m_1, m_2, n_1, and n_2, are given in equation (3.2). This results in the boundary conditions being altered as follows:

$$\text{at}\quad z_1=1\quad (z(c)=1)\text{:}\quad \phi_1=0,\quad \phi_1'=0,\quad \kappa_1=0 \tag{3.11a}$$

$$\text{at}\quad z_2=1\quad (z(b)=1)\text{:}\quad \phi_2=0,\quad \phi_2'=0,\quad \kappa_2=0 \tag{3.11b}$$

$$\text{at}\quad z_1=z_2\ (z_1(a)=z_2(a))\text{:}\quad \phi_1=\phi_2,\quad \phi_1'=\phi_2'\frac{m_2}{m_1},\quad \phi_1''=\phi_2''\frac{m_2^2}{m_1^2},\quad \phi_1'''=\phi_2'''\frac{m_2^3}{m_1^3},\quad \kappa_1=\kappa_2,\quad \frac{m_1}{m_2}\kappa_1'=\kappa_2' \tag{3.11c}$$

As previously done in the base solution, we use a spectral Galerkin technique to solve the resulting system of equations. This is then reduced to a matrix eigenvalue problem

$$\mathbf{A}\mathbf{s}+\beta\,\mathbf{B}\mathbf{s}=\mathbf{0},$$

where β is the temporal eigenvalue and **s** is the eigenvector. The square matrices **A** and **B** depend on the wave number as well as the dimensionless parameters, *Re* and *Sc*. The details of the procedure are given in Appendix B.

CHAPTER 4

RESULTS

Calculations of the stability of incompressible, boundary-free viscous shear flow of similarity form with binary diffusion through the shear layer are described for various values of Schmidt number and the coefficient for viscosity a. Calculations are reported for the basic state, followed by calculations for the stability characteristics of the flow.

4.1 Base State

The effects of a diffusion layer and viscosity variation on the basic state boundary-free shear layer flow were explored by calculations for Schmidt number in the range of $0.1 < Sc < 10.0$, and the coefficient of viscosity, a, of $0.1 < a < 10.0$. The basic state velocity and concentration profiles are presented for the domain size L of 20. The base state profiles do not vary as L is increased as long as it is large enough to allow the limits of the profiles to approach the specified boundary conditions. Therefore, the value of L is not considered when examining the behavior of the base state solution. Later, L will have notable significance when we discuss the stability characteristics of the flow.

Basic state concentration profiles are shown in figures 2 and 3 for the values of Schmidt number of $Sc = 0.1$, 1.0, and 10.0; and for the values of a, $a = 0.1$, 1.0, and 10.0. Note that there is little variation of the concentration profile with varying a for a fixed value of Sc, as shown in figure 3. We also note that the concentration profile becomes

accordingly steeper, approaching a sharp interface, where the value of concentration goes from C_1 to C_2 immediately, as Sc approaches infinity.

The base state velocity profile $u = u(\eta)$, computed for various values of Sc, and a, is shown in figure 4. The velocity profiles change little with Schmidt number for low values of a, while the velocity profile varies significantly for larger values of a. As Sc is increased to 10.0, however, the effects of a almost vanish, and the u velocity profiles are very similar for all values of a. This may indicate as Sc is increased a limiting condition may be approached. The effects of these parameters on the stability of the flow will be explored later. It should be noted that these profiles are computed for $U^* = 0.5$, and $C^* = 0.5$. These parameters will be used throughout, unless otherwise stated.

The effect of varying C^*, and U^*, on the basic state velocity and concentration profiles are illustrated in figures 5 and 6 for $Sc = 1$ and $a = 1$. We note that the u velocity profile changes more gradually and approaches the free stream velocity more slowly for $C^* > 1$, in the region $\eta < 0$. For $C^* < 1$ the velocity profile changes more abruptly than for the case where there is no concentration gradient ($C^* = 1.0$), as shown in figure 5. This can be explained by the fact that the diffusion, in the case of $C^* > 1$, slows the momentum change in the region $\eta < 0$, due to the relation of viscosity with concentration. While, when the direction of the diffusion is reversed ($C^* < 1$) the momentum change is increased in the $\eta < 0$ region due to the lower level of concentration. We also note that the concentration profile changes more gradually for $\eta < 0$ as U^* is increased. This is due to the fact that the increased flow velocity in the $\eta < 0$ region restricting the rate of

diffusion. These results clearly show that the coupling between the base state momentum and diffusion equations is properly occurring. The effect of these trends on the stability of the flow will be discussed later.

4.2 Stability Calculations

The stability code was first tested by stability calculations of laminar jet flow of the form $\hat{u} = U\,\mathrm{sech}^2(\hat{y}/H)$, where H is the half width of the jet and U is the centerline velocity. We first compute the neutral stability curves $Re = Re(\alpha)$ for a fixed value of domain size L, and then determine the critical value of Reynolds number, Re_{cr} at each domain size L that corresponds to the minimum in the neutral stability curve $Re = Re(\alpha)$. For $Re > Re_{cr}(\alpha_{cr})$ the flow is unstable to disturbances in some range of the wavenumber α, while for $Re < Re_{cr}(\alpha_{cr})$ the flow is stable for all values of α.

The critical Reynolds number Re_{cr} and the wave number α_{cr} corresponding to the critical Reynolds number are shown in figure 7 as a function of the domain size L. The critical Reynolds number decreases monotonically as L increases and asymptotically approaches $Re_{cr} = 4$. Similarly, the critical wave number asymptotes to .170 as L increases. These results of $Re_{cr} = 4$ and $\alpha_{cr} = .17$ are in good agreement with the stability results of Tatsumi and Kakutani, 1958. This verifies that the numerical code employed to solve the disturbance equations predicts stability results which are consistent with previous stability reports for laminar jet flow.

The accuracy of spectral-Galerkin-Chebyshev approximation for the eigenvalue problem was tested by checking the spectral convergence of the eigenvalues with the smallest real part. The real part of the least stable eigenvalue is plotted in figures 8, 9 and 10 as functions of the number of polynomials in the expansions shown in Appendix B for various values of α, L, Re and for $Sc = 1$, $U^* = 0.5$, and $C^* = 0.5$. For increasing computational domain size L, and $Re = 1.0$, figure 8 shows the real part of the least stable eigenvalue, $\mathrm{Re}(\beta^*)$ plotted versus N. As shown in figure 8 for $Re = 1.0$, and $\alpha = 0.1$, the $\mathrm{Re}(\beta^*)$ converges for all values of the computational domain size, L, for N of about 15. For $\alpha = 0.001$, the least stable eigenvalue converges to one part in for all L for N of about 20. For $Re = 10.0$, and 100.0 as shown in figure 9, and 10, respectively similar spectral convergence are observed, but it should be noted that the $\mathrm{Re}(\beta^*)$ converges for slightly greater values of N. From these results it is concluded that a value of $N = 30$ is sufficient for use in the stability calculations, and is used to compute neutral stability curves and diagrams presented below.

Regarding dependence of the growth rate, $\mathrm{Re}(\beta^*)$, on the size of the computational domain, L, we again refer to figures 8, 9 and 10. In figure 8 for both $\alpha = 0.1$ and 0.001 it is shown that the spectrally converged values of $\mathrm{Re}(\beta^*)$ do not increase and show any sign of convergence as L is increased. For $Re = 10.0$ and 100.0 the $\mathrm{Re}(\beta^*)$ converges for increasing computational domain size for $\alpha = 0.1$, but does not converge for increasing L for $\alpha = 0.001$, as is shown in figures 9 and 10. From these observations it can be concluded as the value of the wavenumber, α, and the Reynolds number, Re, are

decreased the value of L necessary for convergence of the spectrally converged eigenvalues increases. The implications of this behavior will be shown later to be of major importance when examining the stability of the flow.

The structure of the eigenfunctions corresponding to the disturbance stream function, ϕ, and to the disturbance concentration profile, κ, are shown in figures 11, 12, and 13, for $Re = 10.0$, $Sc = 1.0$, $\alpha = 0.1$, $a = 1.0$, $C^* = 0.5$, $U^* = 0.5$. For computational domain size, $L = 50$ the disturbance stream function is plotted for Chebyshev polynomials $N = 20$, 30, 35, and 40, as shown in figure 11. Both the real, $\mathrm{Re}(\phi)$, and imaginary, $\mathrm{Im}(\phi)$, parts of the disturbance stream function converge as N is increased. It should be noted for $N = 20$ the sign of the eigenfunction is opposite compared to that of the other curves for different values of N. Both ϕ and κ are plotted for $N = 35$ and for different values of the computational domain size, $L = 30$, 40, and 50, as shown in figures 12 and 13. For the eigenfunction ϕ, it is shown in figure 12 that as the computational domain is increased there is no evidence of convergence for the disturbance stream functions, although the shape is consistent. Similar results are observed for the disturbance concentration eigenfunction, κ, in figure 13. It should be noted that for both the real and imaginary parts of ϕ and κ the sign of the eigenfunctions is opposite for $L = 30$; however, the shape is consistent. It can be concluded that for the parameters listed above, the eigenfunctions converge for increasing N, yet do not when changing the size of computational domain. As with the behavior of the eigenvalues, this will be shown to be of importance when investigating the results gathered for the stability of the flow.

The growth rate, the real part of the least stable eigenvalue, $\mathrm{Re}(\beta^*)$, as a function of wavenumber, α, is shown in figure 14 with increasing Reynolds number. Note that the value of $\mathrm{Re}(\beta)$ increases at all values of α, as *Re* is increased, for $L = 40$. Therefore, the flow becomes less stable with increasing *Re,* as is expected. Figure 15 shows similar plots of $\mathrm{Re}(\beta)$ vs α, for $L = 100$. It is apparent that the critical Reynolds number is noticeably less for $L = 100$ than for $L = 40$. This indicates that the size of the computational domain strongly affects the value of Re_{cr}.

From the above findings, we are persuaded to investigate if there is a minimum value of L for which the eigenvalue solutions from the stability equations will converge, similar to what was done in the investigation of the jet flow in section 4.1. To do so, we compute neutral curves for various values of L. These curves are used to determine the stable and unstable regions for the plot of *Re* vs. α. At a fixed *Re*, the values of wavenumber on the neutral curve are found for which the value of $\mathrm{Re}(\beta)$ is equal to zero. In the case of the flows examined in this work, two values of α, for $\mathrm{Re}(\beta) = 0$, are found for each *Re* above the critical Reynolds number. These points are plotted for a number of different *Re*, and formed into curves. The curve of the lower values of α are known as the lower branch, and likewise, the larger α curve is the upper branch. The location where these curves meet determines the minimum point for the entire neutral curve, and yields Re_{cr}. Likewise, the corresponding value of α at this minimum is referred to as α_{cr}. We first choose the case with constant viscosity ($a = 0$) and create neutral curves (*Re* vs. α) for different values of L. For $L = 50$, figure 16 illustrates the plot of the neutral curve.

Here, the stable and unstable regions are labeled, as well as Re_{cr}, α_{cr}, the lower and upper branches.

In figure 17 it is shown as the value of L increases, the neutral curve becomes larger at the lower limit, or rather the values of α for $\mathrm{Re}(\beta) = 0$ are smaller for corresponding Re. The limit of α for stability at a given Reynolds number varies inversely with L. This trend indicates that there is not a non-zero Reynolds number where the flow will be stable for all values of α, and that the flow must be unstable for all Re. This trend of Re_{cr} and the corresponding wave number α_{cr} approaching zero with the value of $L \rightarrow \infty$ is shown in Figure 18. It will be shown later that similar behavior will be observed for the variable viscosity case as well.

Although, it appears that the stability calculation here does not predict a non-zero critical Reynolds number exists, neutral curves are plotted to view the effects of viscosity and concentration parameters on stability of the flow. The neutral curves for a of 0.1, and 1.0 are plotted for Sc values of 0.1, 1.0, and 10.0, with L equal to 40 in Figure 19. For $a = 0.1$ there is almost no change in the neutral curves when comparing Sc values of 0.1 and 1.0, as these curves are almost identical. As the Schmidt number is increased to 10.0, it is apparent that the flow becomes less stable; as Re_{cr} decreases to about 1.6. It should be noted, however, that the upper limit, which the neutral curve converges to as L grows, changes very little with Sc, as might be expected for a relatively small value of a. It is observed that for larger values of a the effects of Sc are more pronounced. From $a =$ 0.1, to 1.0 for $Sc = 0.1$, Re_{cr} actually decreases, while at $Sc = 1.0$, Re_{cr} remains nearly the

same. For $Sc = 10.0$, Re_{cr} decreases considerably for larger values of a, and the upper limit does show an increase in the unstable region.

The neutral curves are plotted for $a = 1.0$, $Sc = 1.0$, $U^* = 0.5$, $C^* = 0.5$, and $L =$ 40, 50, and 100 in figure 20, to illustrate the effect of increasing domain size. For the lower branch, the curve approaches $\alpha = 0$ for all Re as L is increased. For the upper portion the curve converges to relatively the same solution for all values of L. This is similar to the behavior for the constant viscosity case. From this behavior it is apparent that for variable viscosity as a function of c, Re_{cr} is zero, as was the case for constant viscosity.

The effect of ratios of far-field velocities and concentrations at each end, $U^* = 0.5$ and $C^* = 0.5$, on the stability of boundary free shear flows is examined next. The behavior of the upper neutral curves are observed for $U^* = 0$, and $C^* = 0.5$ in figure 21. Here, the curves are compared to those using the original condition, $U^* = 0.5$ and $C^* = 0.5$, for $a =$ 1.0, and $Sc = 0.1$, 1.0, and 10.0. There is not a drastic difference in the shape of the neutral curve from that of the $U^* = 0.5$ case. The behavior is similar for all values of Sc examined. It is evident form this that the u velocity profile shape does not have a major impact on the stability characteristics of the shear flow we are examining. This is concordant with the fact that for flows with inflection points in the velocity profile, as the one we are examining, the neutral stability curve is found to be somewhat insensitive to the shape of the main velocity profile, u.

Next, the neutral curves with the initial condition $C^* = 2.0$ are compared to those of $C^* = 0.5$, to examine the change in the stability behavior when altering the concentration profile. It is observed in figure 22 that for $Sc = 0.1$ and 1.0 the flow is more stabilized for $C^* = 2.0$ when compare to the curve for $C^* = 0.5$. This is due to the curves for $C^* = 2.0$ are made up of lower values of α for corresponding Re, when compared to the curves for the $C^* = 0.5$. However, when Sc is increased to 10.0 the neutral curve reveals that the flow appears less stable for $C^* = 2.0$ when compared to $C^* = 0.5$. These findings may indicate that for values of Sc of unity or less the diffusion of particles in the direction of the lower velocity limit actually creates a more stable flow than when the particles diffuse toward the larger limit of free stream velocity. For the case where diffusion has a greater impact on stability than momentum ($Sc > 1$); however, this change in diffusion direction magnifies infinitesimal disturbances.

CHAPTER 5

DISCUSSION

The results presented in Chapter 4 illustrate the base state as well as the stability behavior of this flow field with varying parameters. The major results of the stability analysis lead us to consider an explanation for these findings.

The major finding is that the Re_{cr} was equal to zero, for the flow studied. This agrees with the previous findings for a boundary-free shear flow without transport of species due to a concentration gradient. This trend is consistent with the fact that the flow appears to be destabilized with increasing effects of a concentration gradient, or more explicitly increasing Sc. Therefore, it would not be expected that the effects of concentration would give way to the flow having a non-zero critical Reynolds number. From a physical point of view, these results can be explained by the fact that the transport of species through the shear layer may serve as an additional disturbance causing mechanism, where diffusion must excite rather than dampen infinitesimal disturbances. However, it should be noted that for $Sc < 1$, there is a destabilizing effect as the level of viscosity influence grows, or rather as a is increased. This would indicate that for cases where the velocity profile influences stability, $Sc < 1$, viscosity effects tend to stabilize the flow. Yet, where the instability is more strongly influenced by the concentration layer, the effect of viscosity is to cause the flow to be more unstable. This is consistent with the fact that viscosity is known to have a dual nature, where its effects are known to be diffusive as well as dissipative.

Another noteworthy observation concerns the trend of stability with changes in the velocity profile. Although, only one comparison is made with the effect of the freestream velocity ratio, U^*, on the neutral-stability curve, the observed trend is in agreement with previous results. For velocity profiles with inflection points, the shape of the stability curve is known to be insensitive to the changes in shape of the velocity profile. In addition, the slight variation that was observed may be attributed to the minor change in the concentration profile that occurs with a change in U^*.

The effect of varying the concentration ratio, C^*, on the stability, is observed as well. For $Sc \leq 1$ it was shown that the flow is stabilized when increasing C^* from 0.5 to 2.0. However, for $Sc = 10$ the flow becomes destabilized for this same change in C^*. This may be attributed to the fact that for $Sc \leq 1$ the velocity profile is driving the stability and the change in u with the change in C^* is responsible for the observed stability trend. Yet, when Sc is increased further the concentration profile now more strongly governs stability of the flow. This would indicate as the direction of the transport of the species is changed from going into the slower moving fluid, $U^* = 0.5$, $C^* = 0.5$, to going into the faster moving fluid, $U^* = 0.5$, $C^* = 2.0$, the flow becomes less stable.

It is apparent that the findings discussed above may have been better understood if the flow field studied had a finite Re_{cr}. The change in the stability of the flow could have been analyzed by not only examining the change in shape of the stability curves, but by also observing the changes in Re_{cr} as different parameters were examined. A suggestion for further study is to examine the stability behavior of the viscosity variation with concentration in a jet flow. The jet fluid would have a different concentration level than

the stationary medium. This was attempted; however, it was not possible to solve for the base concentration profile in the jet. With the known boundary conditions, the concentration equations derived in conjunction with the similarity solution for the jet flow did not adequately predict the diffusion within the jet.

Another aspect of the problem that may have to be explored is to not assume parallel flow in the stability analysis. Due to the fact that we are concerned with flows of low *Re* for boundary-free flows, the assumption that v(y) is much less than $u(y)$ may be invalid. Although, the inclusion of the y-direction velocity in the stability analysis may considerably complicate the problem, it may prove necessary in accurately predicting the stability characteristics of the flow. Therefore the results and conclusions of this report should be observed with this in mind.

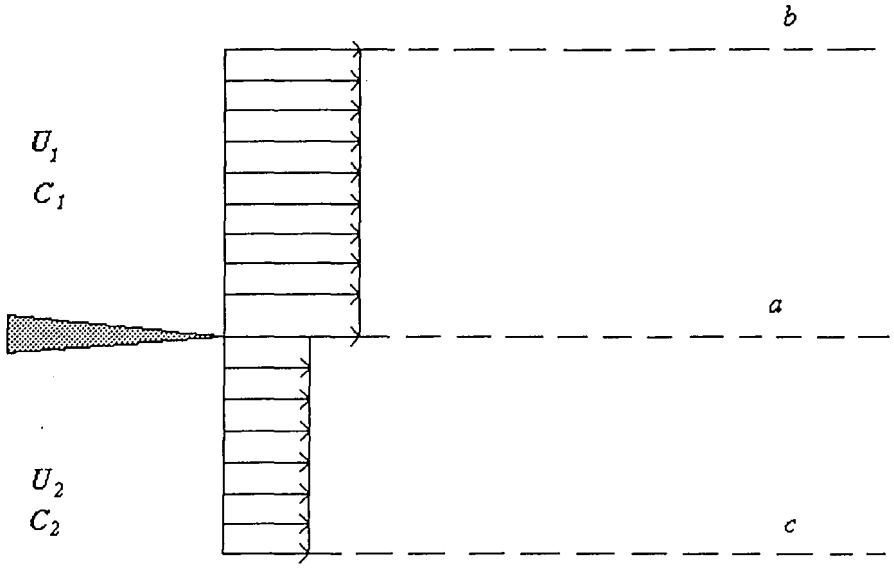

Figure 1. Schematic of boundaries for truncation of domain

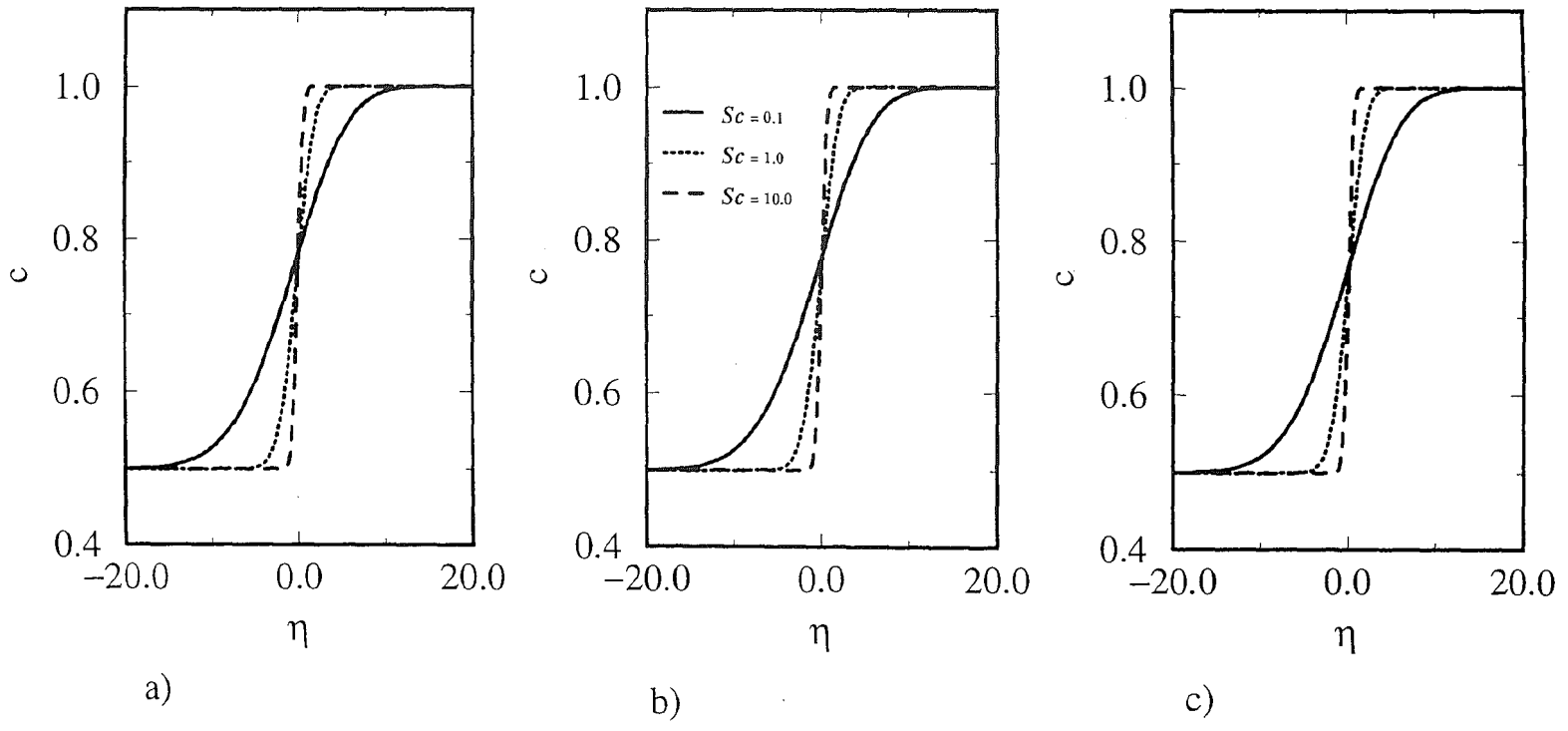

Figure 2. Basic state concentration profiles, computed for free shear flows for $U^* = 0.5$, and $C^* = 0.5$ and the values of Schmidt number $Sc = 0.1, 1.0, 10.0$. Results are presented for a) $a = 0.1$, b) $a = 1.0$, and c) $a = 10.0$.

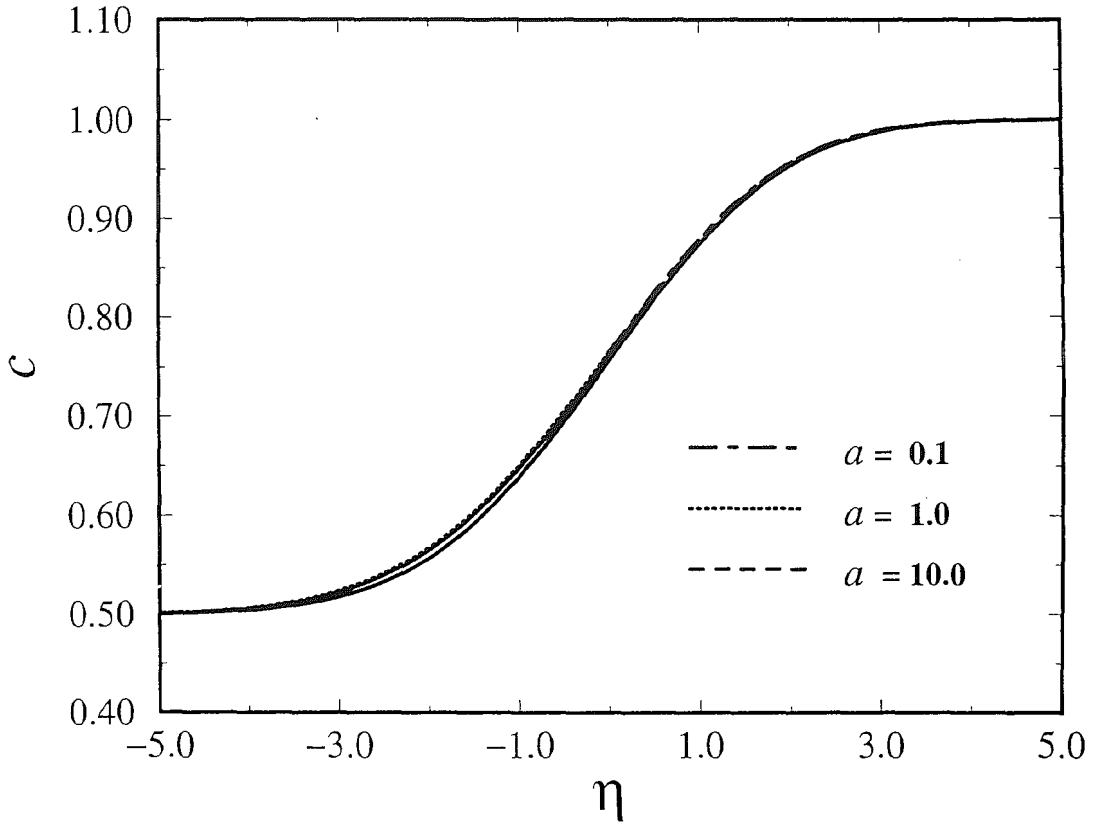

Figure 3. Basic state concentration profiles for $Sc = 1.0$, $U^* = 0.5$, $C^* = 0.5$, $a = 0.1$, 1.0, and 10.0.

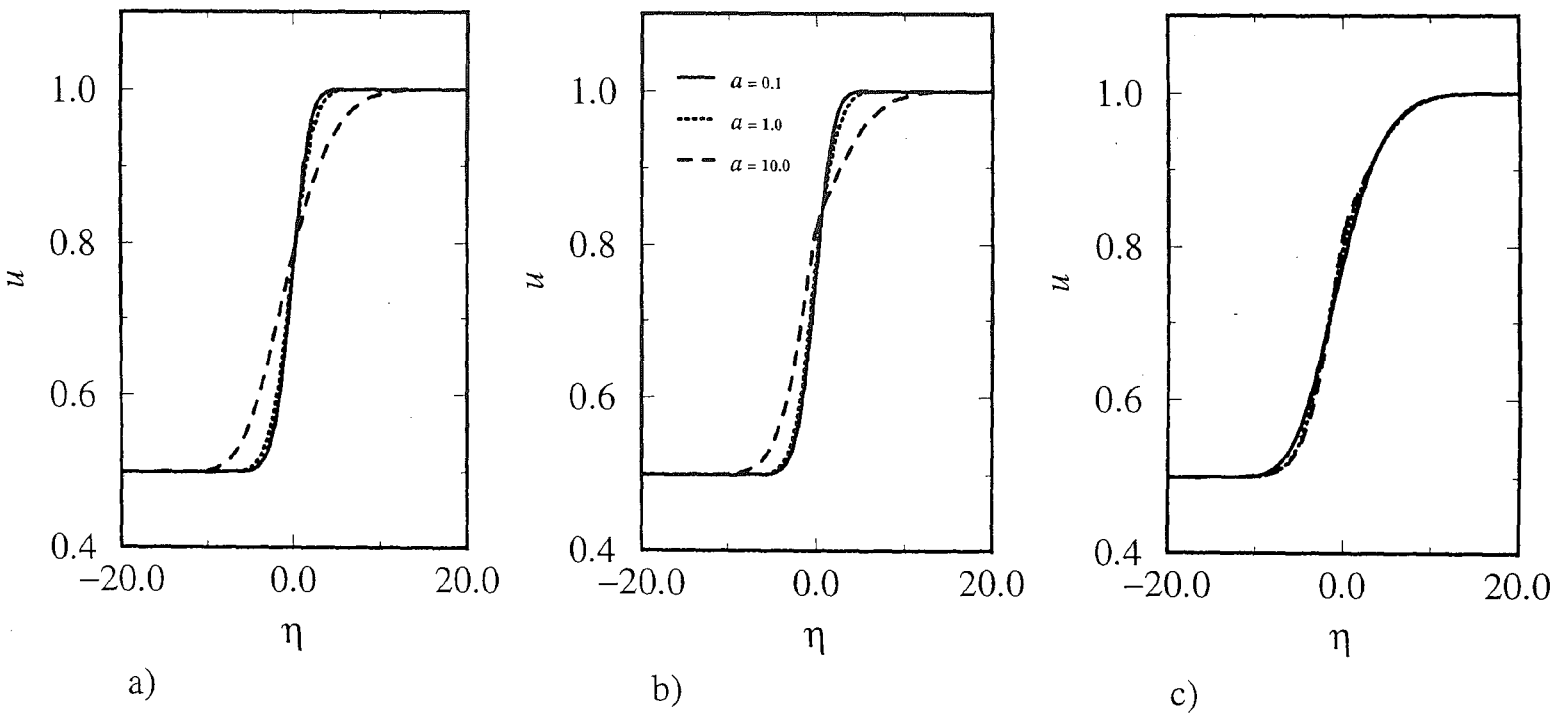

Figure 4. Basic state velocity profiles computed for free shear flows for $U^* = 0.5$, $C^* = 0.5$, and the values of $a = 0.1$, 1.0, and 10.0. Results are presented for a) $Sc = 0.1$, b) $Sc = 1.0$, and c) $Sc = 10.0$.

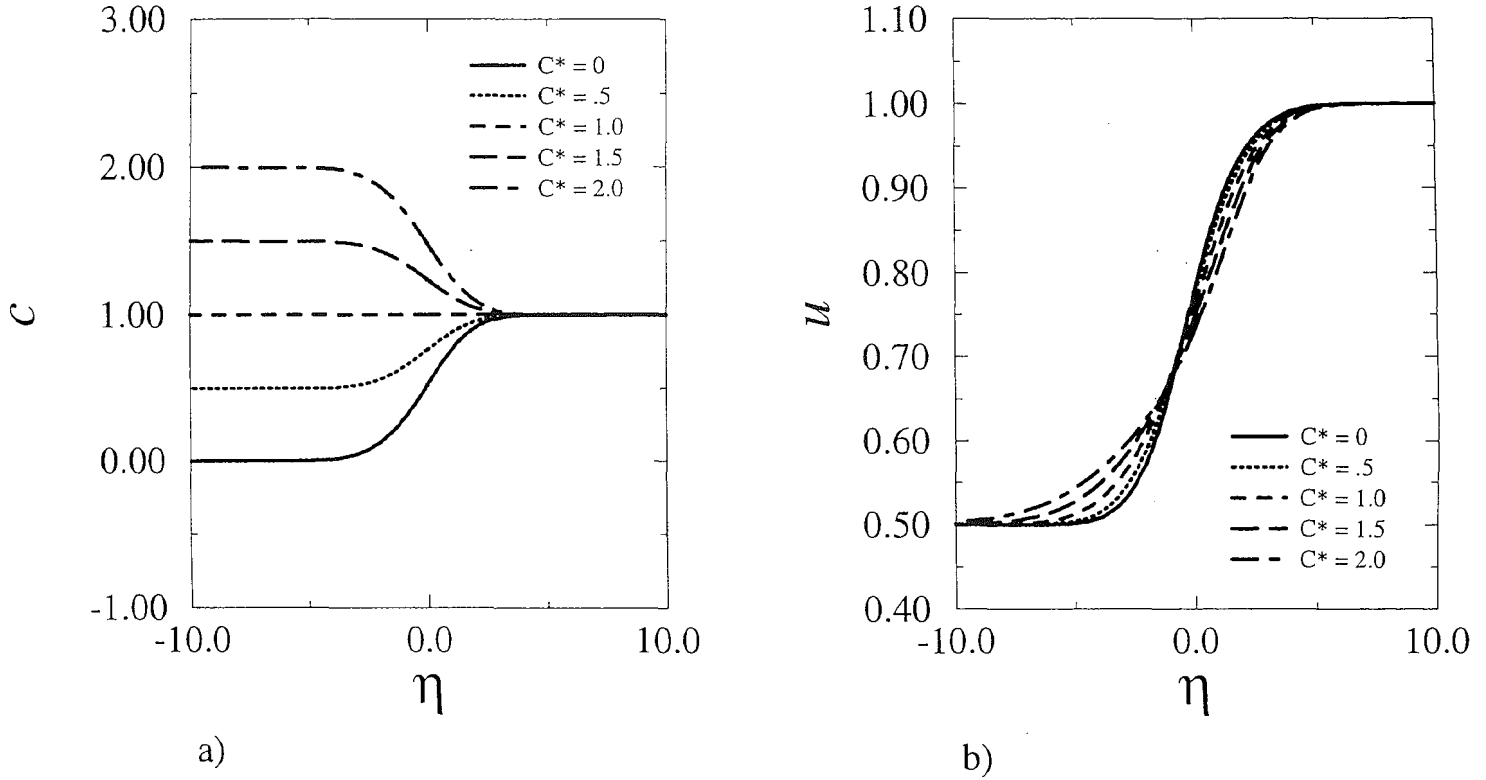

Figure 5. a) Basic state concentration profiles and b) Basic state velocity profiles for $a = 1.0$, $Sc = 1.0$, and $U^* = 0.5$ and various values of the ratio of far field concentrations at each end, C^*.

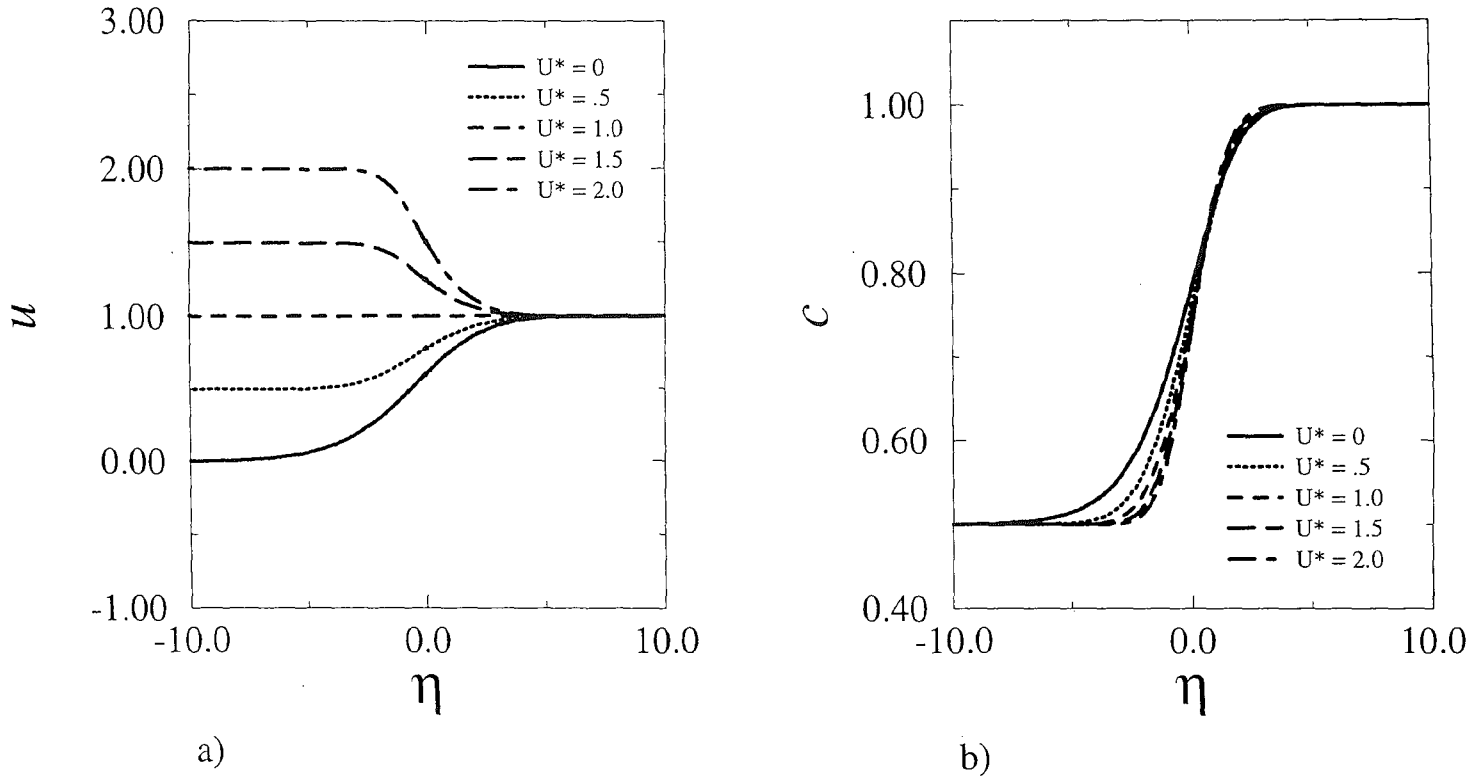

Figure 6. a) Basic state velocity profiles and b) basic state concentration profiles for $a = 1.0$, $Sc = 1.0$, and $C^* = 0.5$ and various values of the ratio of far field velocities at each end, U^*.

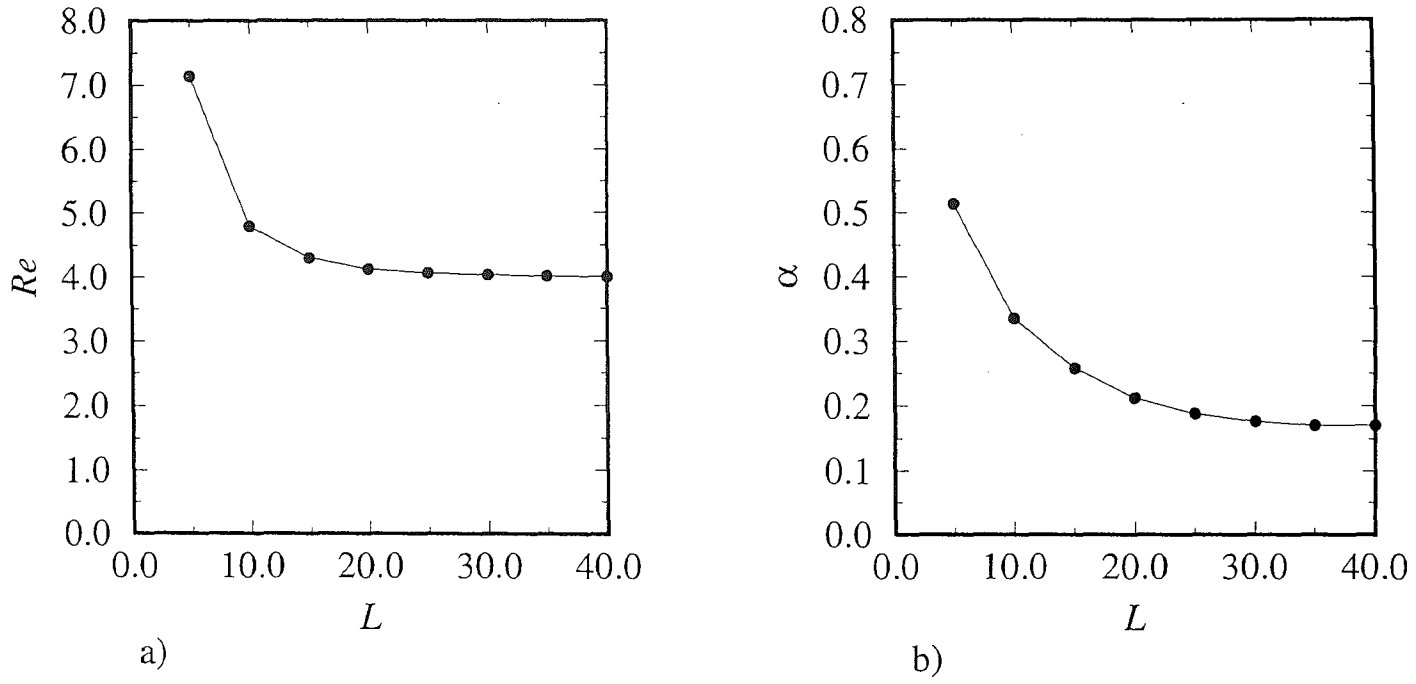

Figure 7. Stability boundaries a) $Re_{cr} = Re_{cr}(L)$ and b) $\alpha_{cr} = \alpha_{cr}(L)$ computed for jet flow with hyperbolic tangent velocity profile $u = \text{sech}^2(y)$.

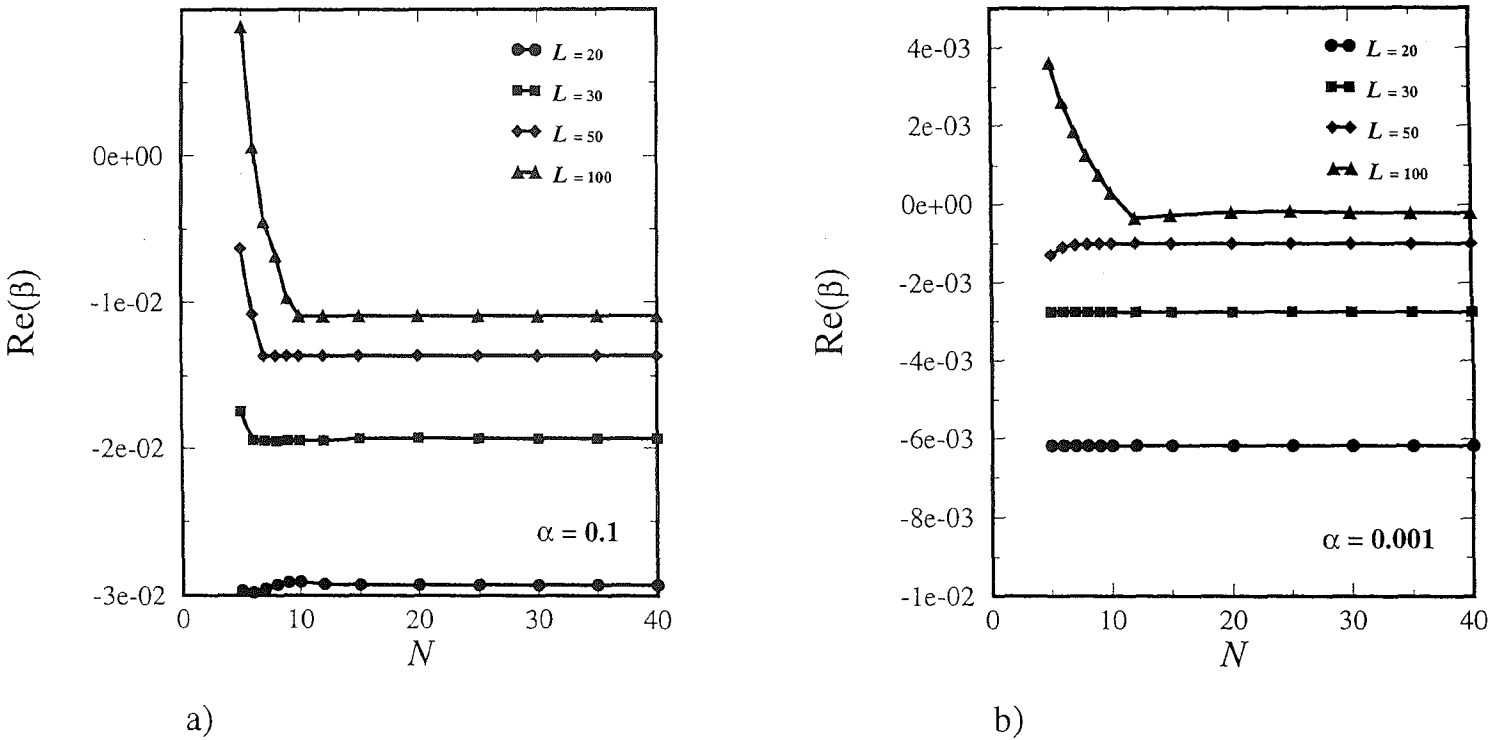

Figure 8. Real part of the least stable eigenvalue β^*, Re(β^*), vs. N computed for $Re = 1.0$, $a = 1.0$, $Sc = 1.0$, $U^* = 0.5$, $C^* = 0.5$, and computational domain sizes of $L = 20$, 30, 50 and 100. Results are presented for a) $\alpha = 0.1$ and b) $\alpha = 0.001$.

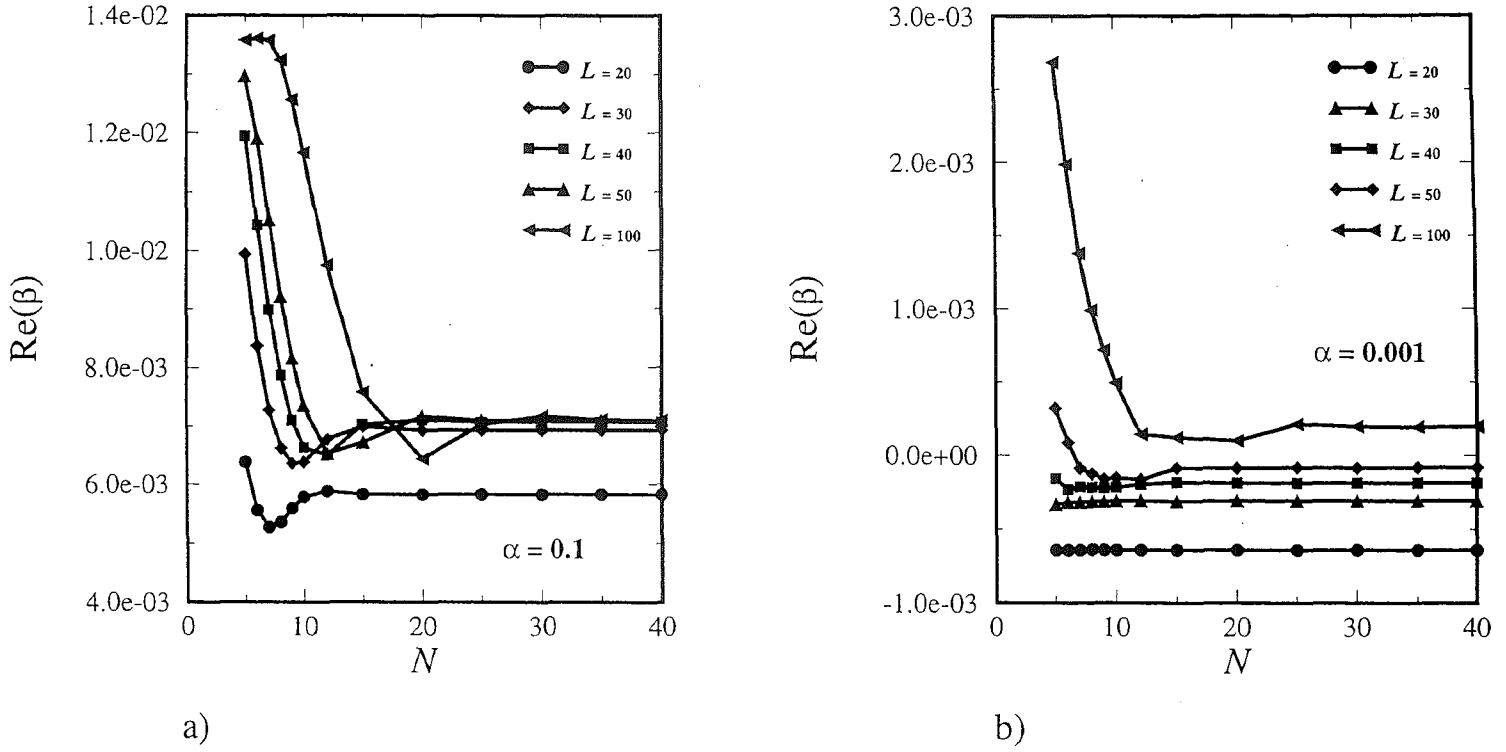

Figure 9. Real part of the least stable eigenvalue β^*, Re(β^*), vs. N computed for Re = 10.0, a = 1.0, Sc = 1.0, U^* = 0.5, C^* = 0.5, and computational domain sizes of L = 20, 30, 50 and 100. Results are presented for a) α = 0.1 and b) α = 0.001.

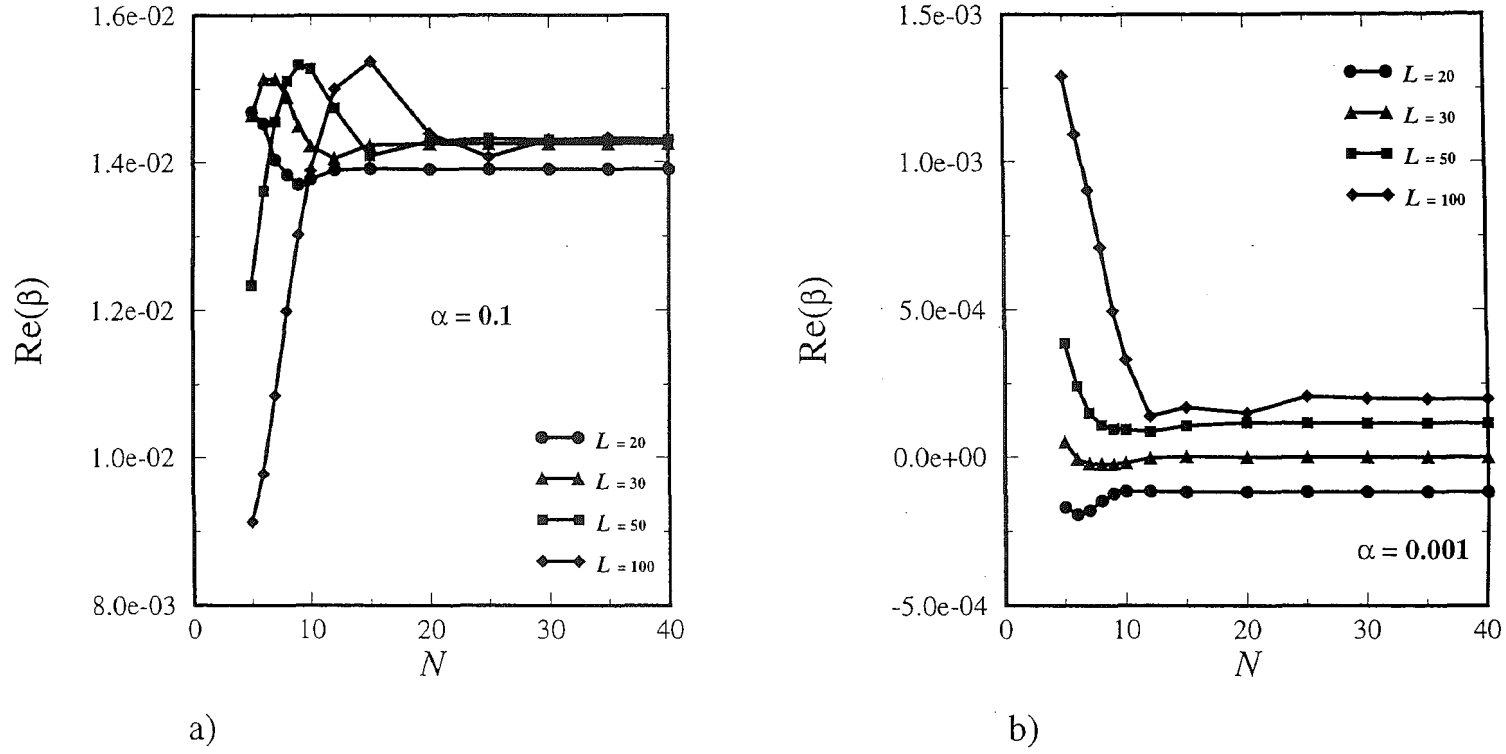

Figure 10. Real part of the least stable eigenvalue β^*, Re(β^*), vs. N computed for Re = 100.0, a = 1.0, Sc = 1.0, U^* = 0.5, C^* = 0.5, and computational domain sizes of L = 20, 30, 50 and 100. Results are presented for a) α = 0.1 and b) α = 0.001.

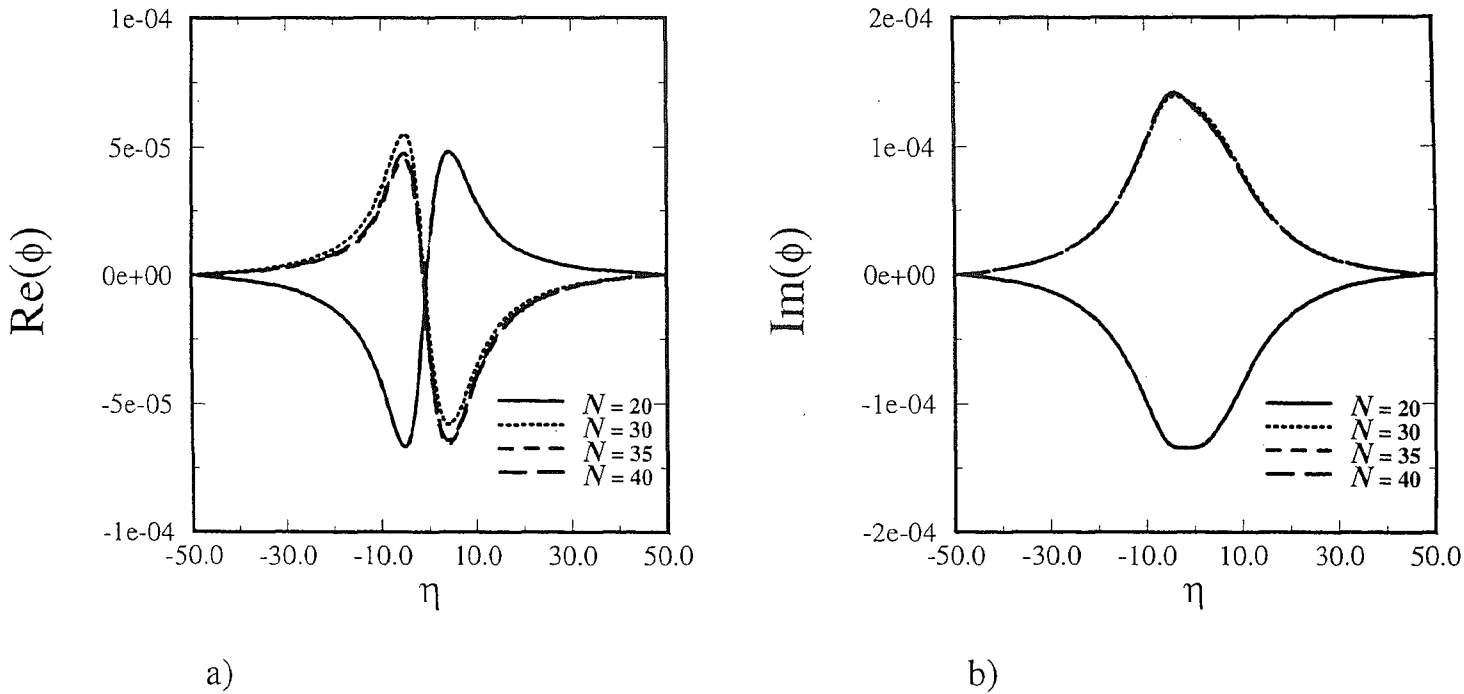

Figure 11. Disturbance stream eigenfunction $\phi = \phi(\eta)$, a) Real part and b) Imaginary part. Results presented for Chebyshev polynomials, $20 \leq N \leq 40$, with $Re = 10.0$, $Sc = 1.0$, $\alpha = 0.1$, $a = 1.0$, $C^* = 0.5$ and $U^* = 0.5$.

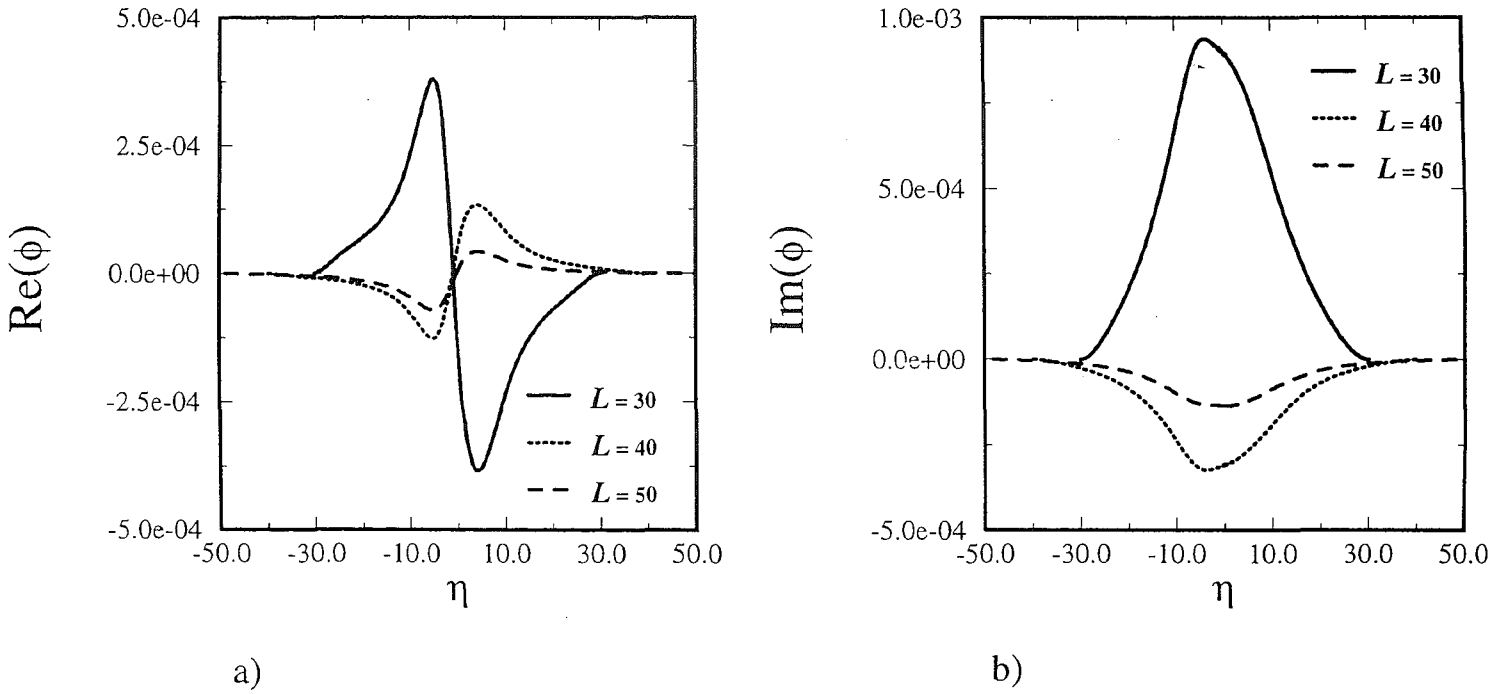

Figure 12. Disturbance stream eigenfunction $\phi = \phi(\eta)$, a) Real part and b) Imaginary part. Results presented for computational domain size, $30 \leq L \leq 50$, with $Re = 10.0$, $Sc = 1.0$, $\alpha = 0.1$, $a = 1.0$, $C^* = 0.5$ and $U^* = 0.5$.

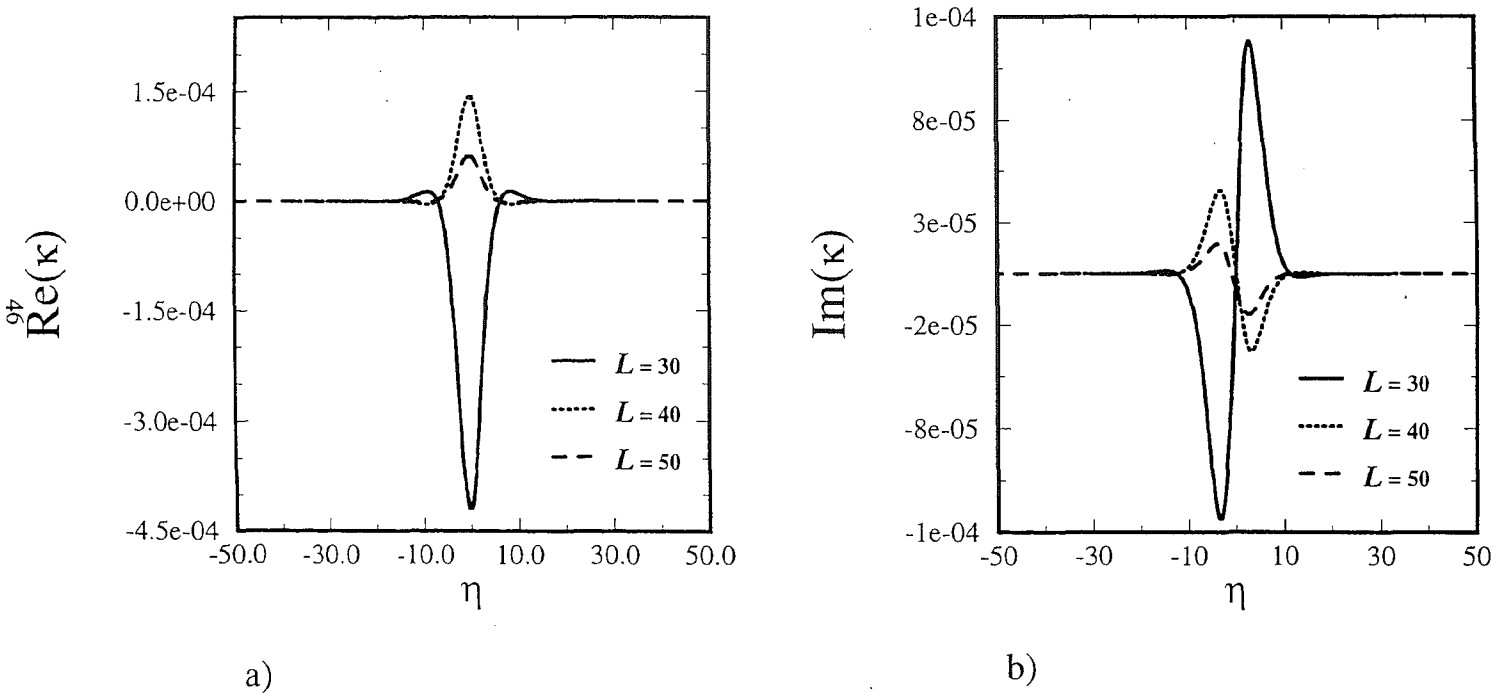

Figure 13. Disturbance concentration eigenfunction $\kappa = \kappa(\eta)$, a) Real part and b) Imaginary part. Results presented for computational domain size, $30 \leq L \leq 50$, with $Re = 10.0$, $Sc = 1.0$, $\alpha = 0.1$, $a = 1.0$, $C^* = 0.5$ and $U^* = 0.5$.

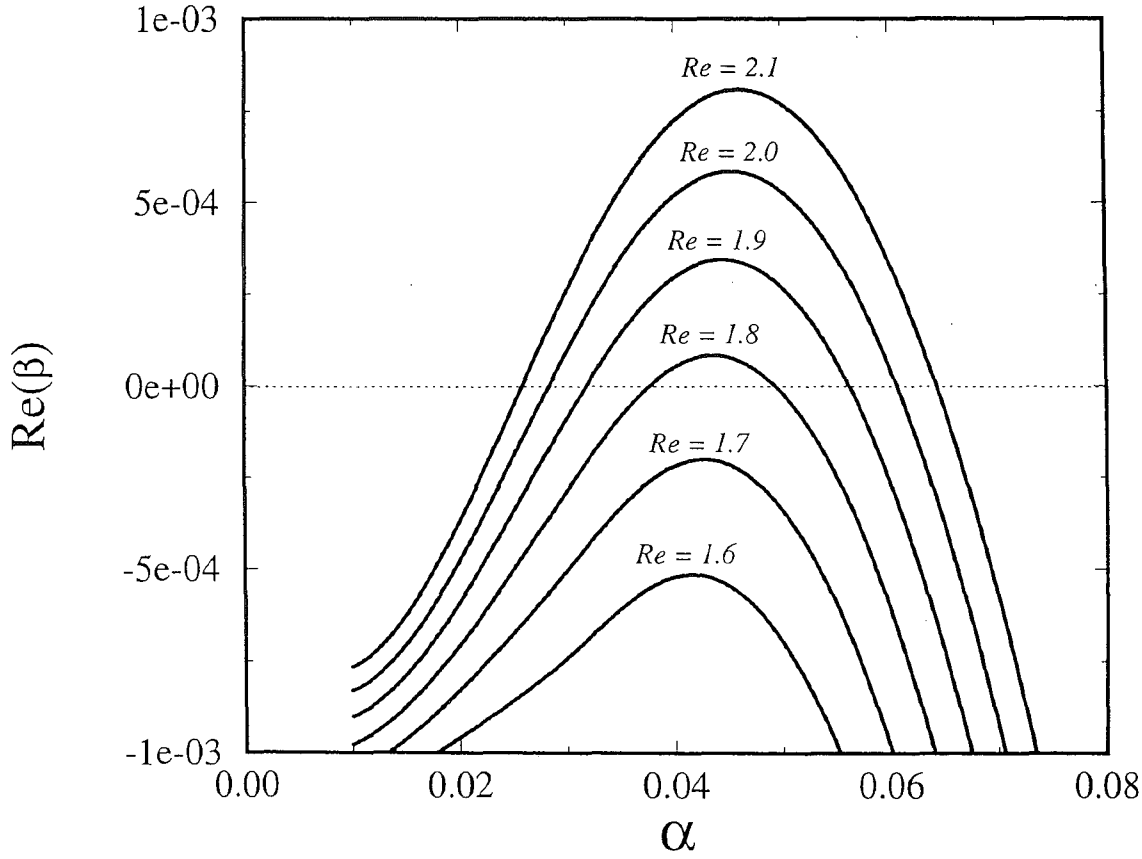

Figure 14. Growth rate, Re(β^*) vs. wave number, α, for $L = 40$, $a = 1.0$, $Sc = 1.0$, $U^* = 0.5$, $C^* = 0.5$, and the range of Reynolds number, $1.6 \leq Re \leq 2.1$.

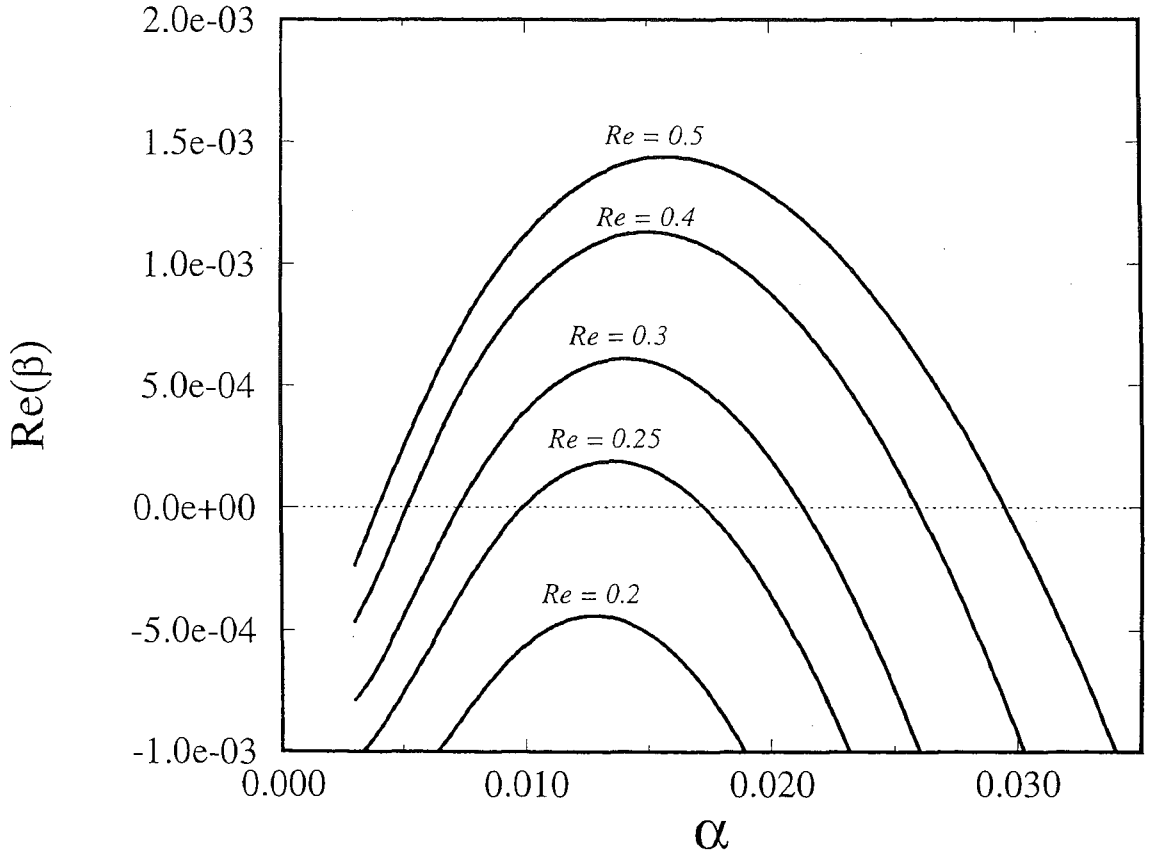

Figure 15. Growth rate, Re(β^*) vs. wave number, α, for $L = 100$, $a = 1.0$, $Sc = 1.0$, $U^* = 0.5$, $C^* = 0.5$, and the range of Reynolds number, $0.2 \leq Re \leq 0.5$.

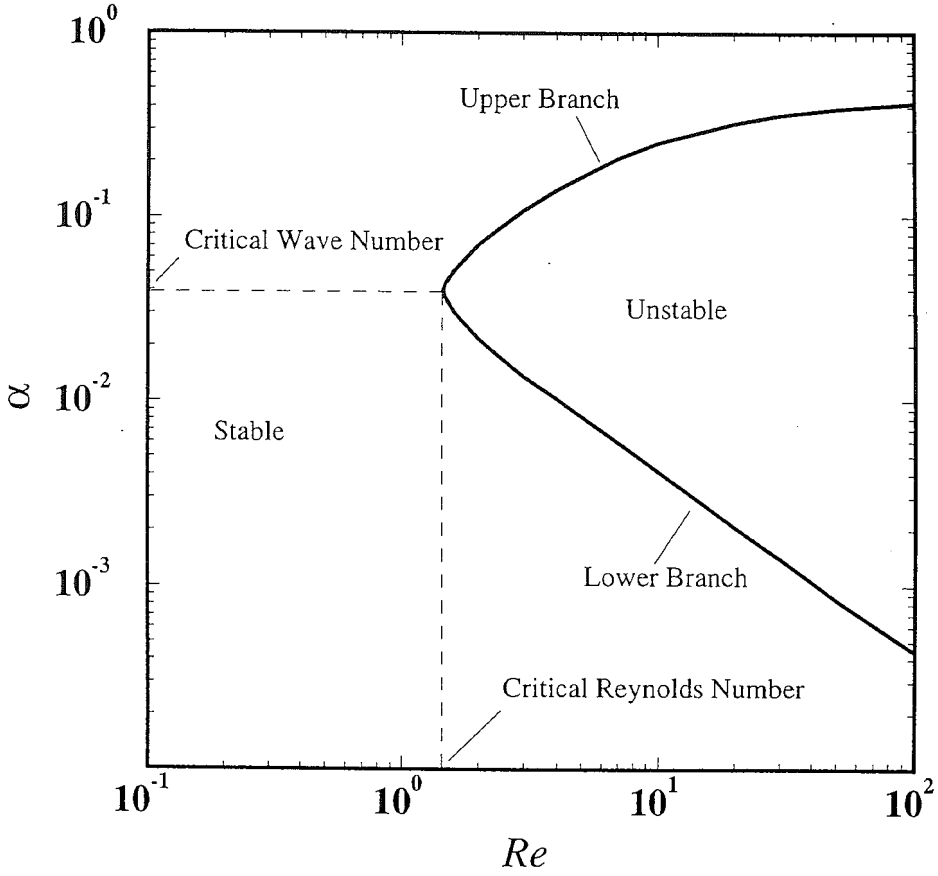

Figure 16. Neutral Stability Curve $Re = Re(\alpha)$ illustrating stable and unstable regions, critical wave number and Reynolds number, and lower and upper branch. Plotted for $L = 50$, $a = 0$, $U^* = 0.5$ and $C^* = 0.5$.

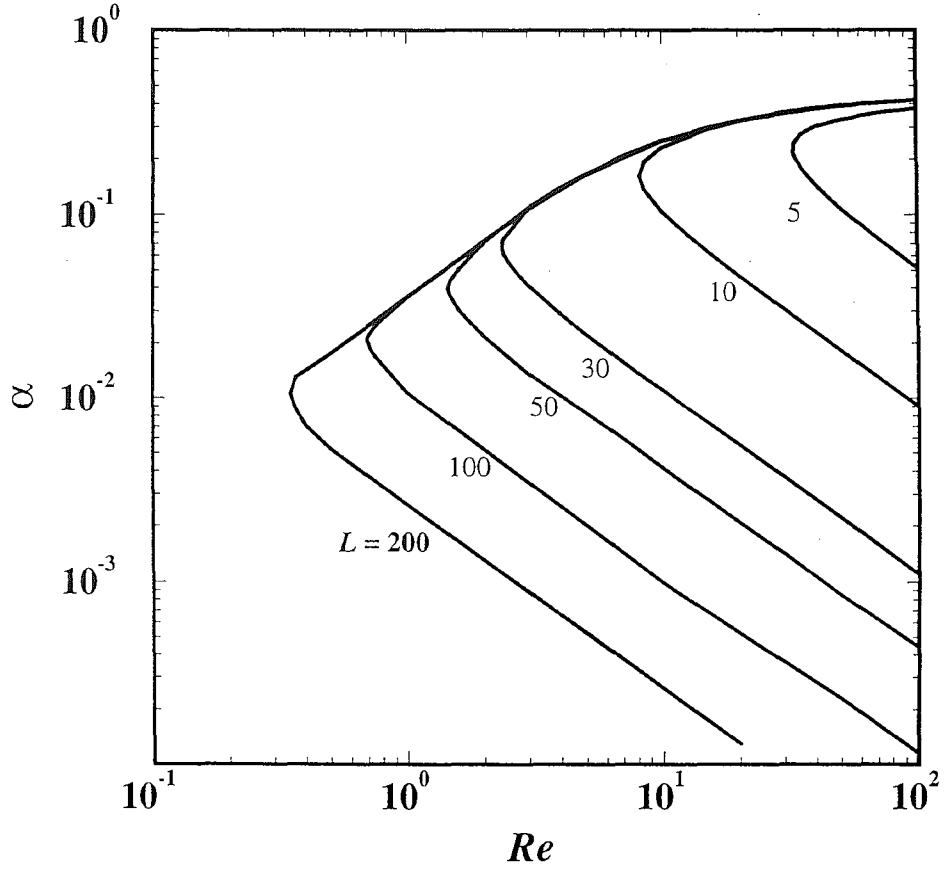

Figure 17. Neutral stability curves $Re = Re(\alpha)$ for computational domain sizes, $5 \leq L \leq 200$. Plotted for $a = 0$, $U^* = 0.5$ and $C^* = 0.5$.

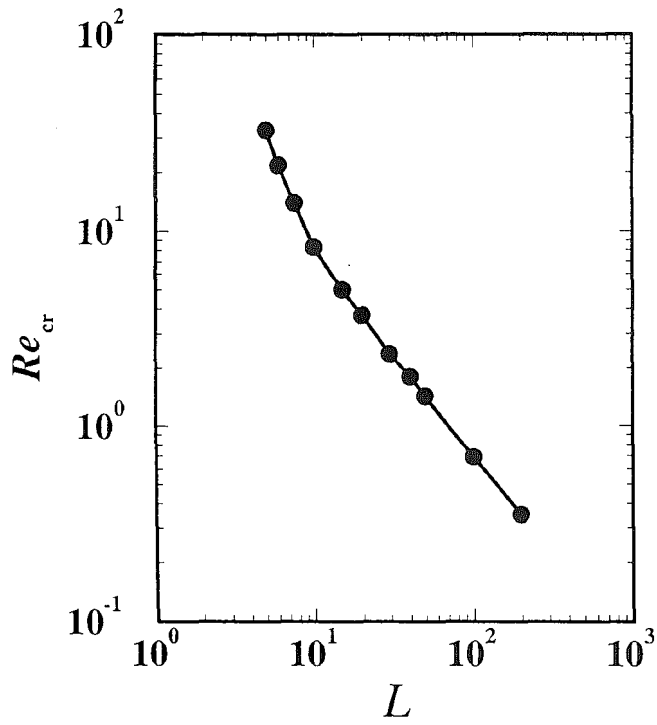

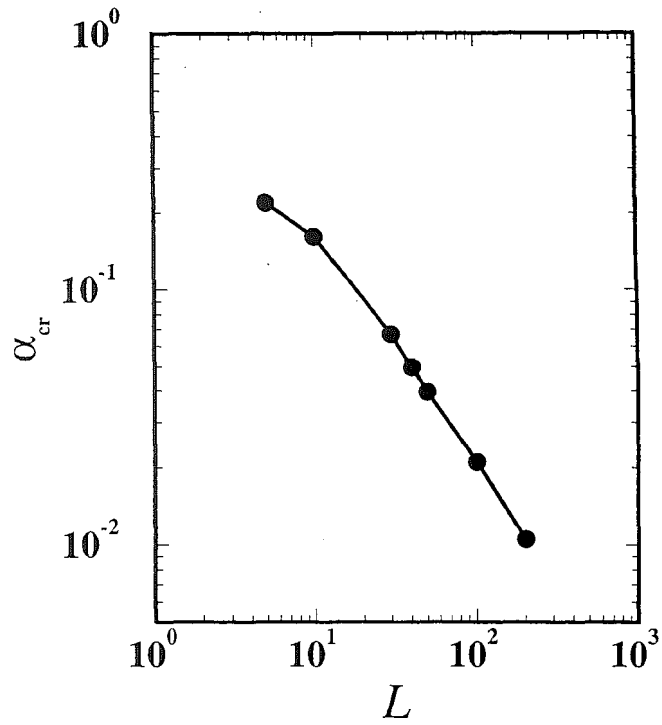

Figure 18. Stability boundaries a) $Re_{cr} = Re_{cr}(L)$ and b) $\alpha_{cr} = \alpha_{cr}(L)$ computed for $a = 0$, $U^* = 0.5$ and $C^* = 0.5$.

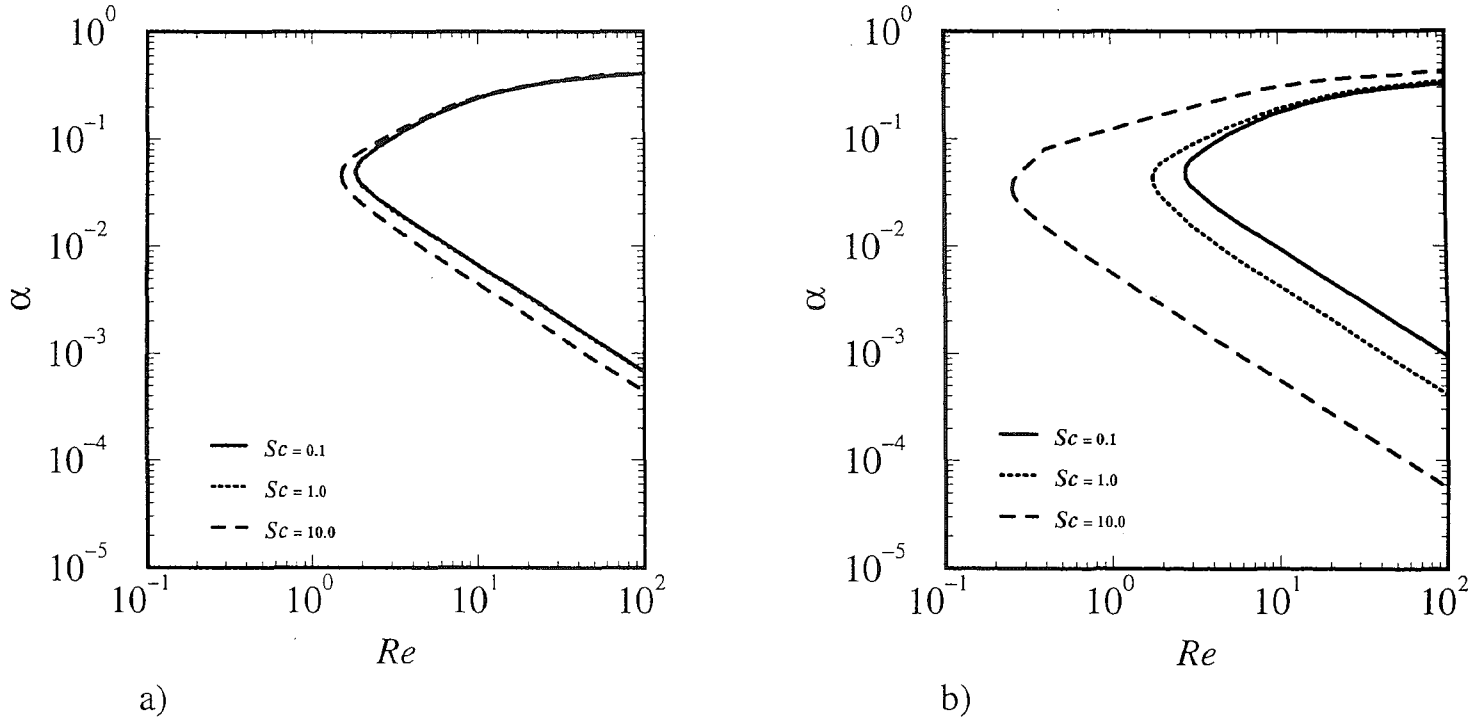

Figure 19. Neutral stability curves $Re = Re(\alpha)$ computed for $U^* = 0.5$, $C^* = 0.5$ and various values of Schmidt number, $Sc = 0.1$, 1.0, and 10.0. Results shown for a) $a = 0.1$ and b) $a = 1.0$.

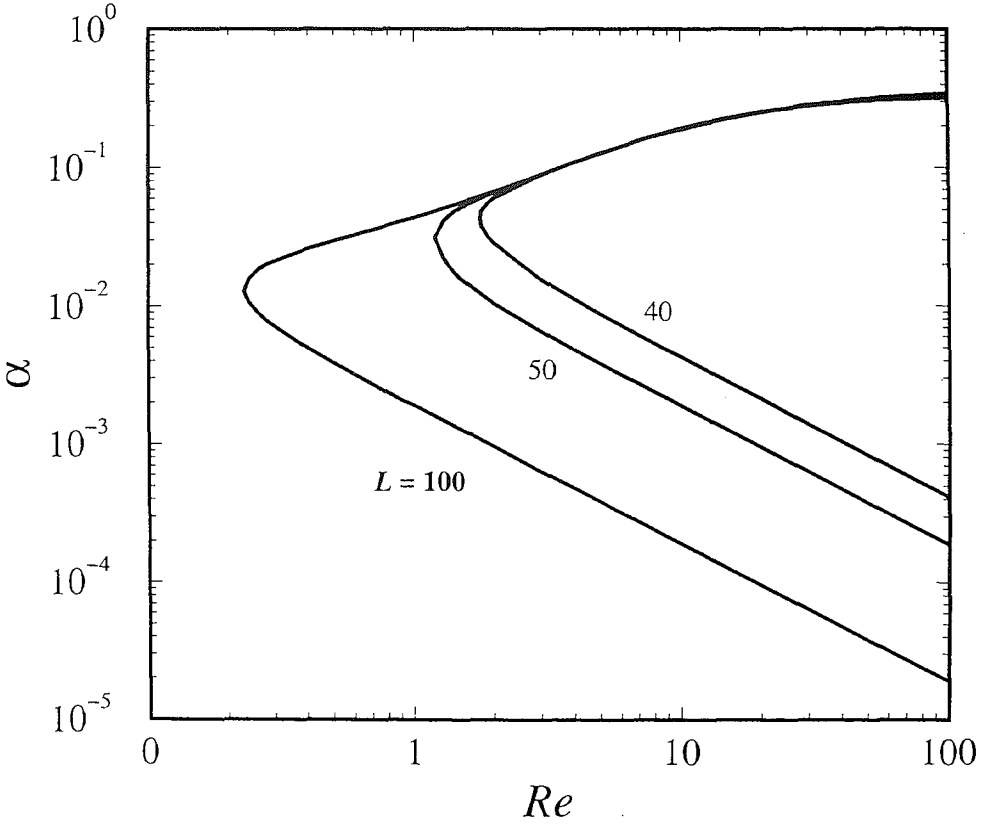

Figure 20. Neutral stability curves $Re = Re(\alpha)$ computed for $U^* = 0.5$, $C^* = 0.5$ and various values of computational domain size, L = 40, 50 and 100.

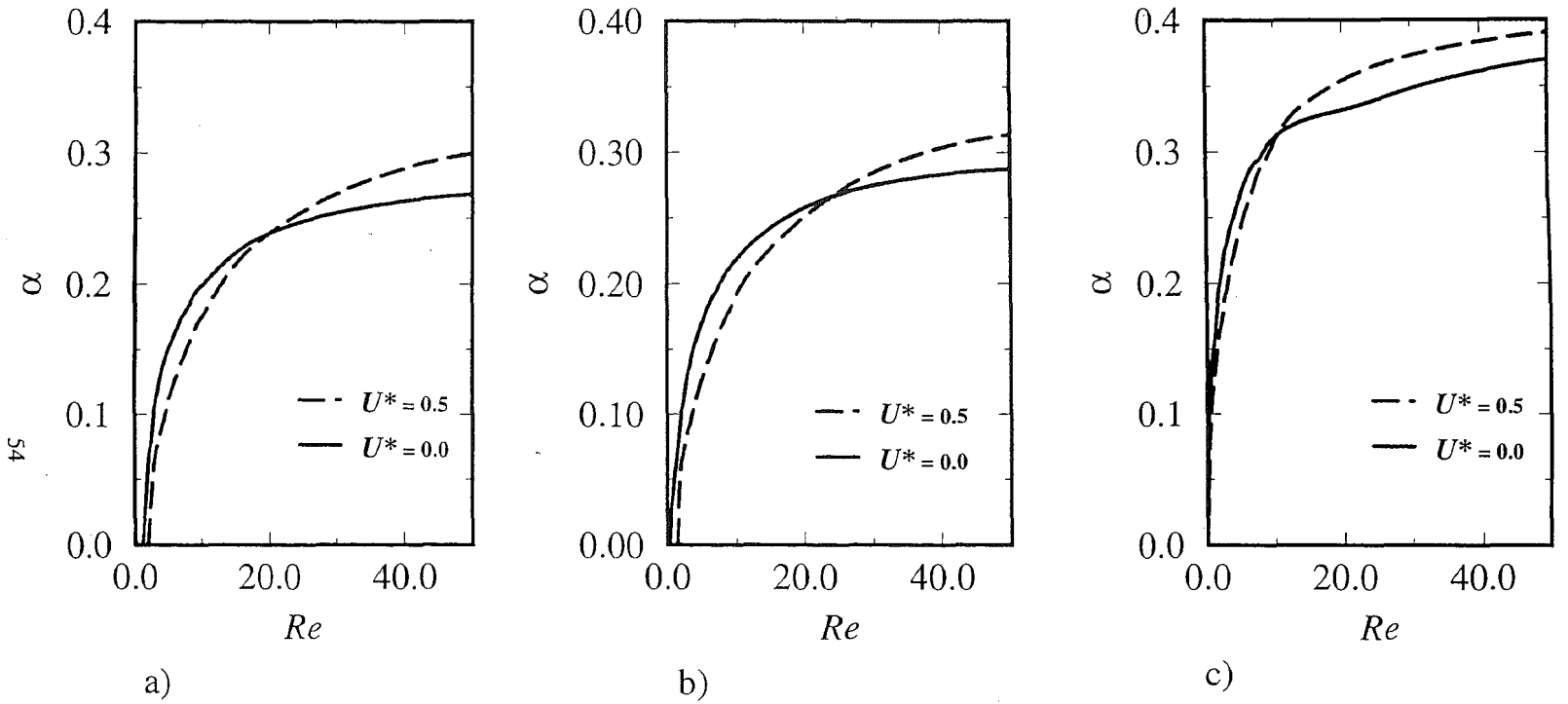

Figure 21. Upper branch of neutral stability curves $Re = Re(\alpha)$ for $U^* = 0.0$, and 0.5, $a = 1.0$, $L = 40$, and $C^* = 0.5$. Computed for a) $Sc = 0.1$, b) $Sc = 1.0$, and c) $Sc = 10.0$.

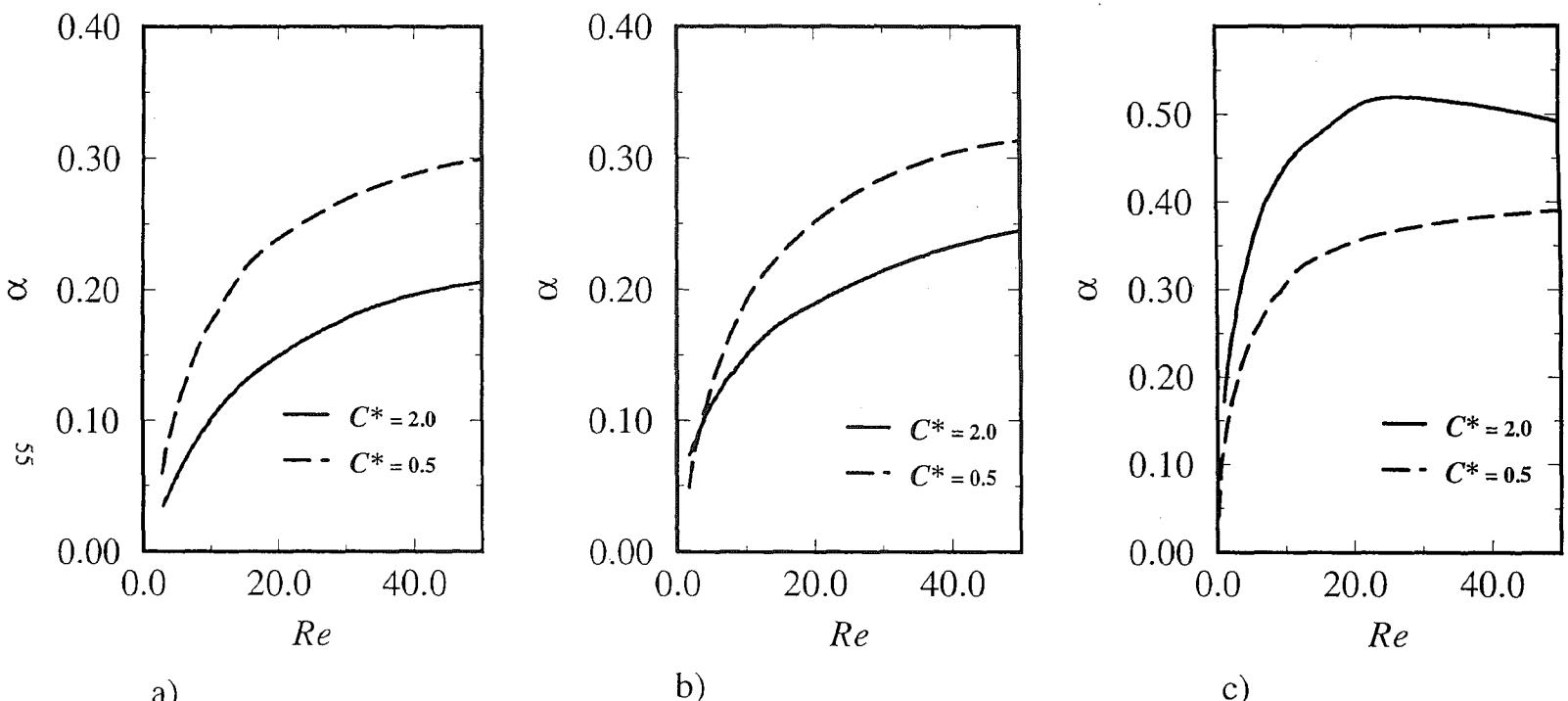

Figure 22. Upper branch of neutral stability curves $Re = Re(\alpha)$ for $C^* = 0.5$, and 2.0, $a = 1.0$, $L = 40$, and $U^* = 0.5$. Computed for a) $Sc = 0.1$, b) $Sc = 1.0$, and c) $Sc = 10.0$.

References

Azaiez, J. & Homsy, G.M. 1993 Linear stability of free shear flow of viscoelastic liquids. *J. Fluid Mech.* **268**, 37-69.

Azaiez, J. 1993 *Instability of Newtonian and non-Newtonian Free Shear Flows*. Ph.D. Thesis, Stanford University.

Balsa, T. F. 1987 On the spatial instability of piecewise linear free shear layers. *J. Fluid. Mech.* **174**, 553-563.

Betchov, R. & Criminale, W. O. 1967 *Stability of Parallel Flows*. Academic Press, New York.

Betchov, R. & Szewczyk, A. 1963 Stability of a shear layer between parallel streams. *Physics of Fluids.* **6** (10), 1391-1396.

Drazin, P. G. & Howard, L.N. 1962 The instability to long waves of unbounded parallel inviscid flow. *J. Fluid. Mech.* **14**, 257-283.

Incropera, F. P. & DeWitt, D. P. 1990 *Fundamentals of Heat and Mass Transfer*. John Wiley and Sons, New York.

Ling, C. & Reynolds, W.C. 1972 Non-parallel flow corrections for the stability of shear flows. *J. Fluid. Mech.* **59**, 571-591.

Lock, R. C. 1951 The velocity distribution in the laminar boundary layer between parallel streams. *Quart. Journ. Mech. and Applied Math.* **4** (1), 42-63.

Metcalfe, R. W., Orzag, S. A., Brachet, M. E., Menon, S. & Riley, J. J. 1987 Secondary instability of a temporally growing mixing layer. *J. Fluid Mech.* **184**, 207-243.

Michalke, A. 1964 On the inviscid instability of the hyperbolic-tangent velocity profile. *J. Fluid Mech.* **19**, 543-556.

Panton, R. L. 1984 *Incompressible Flow*. John Wiley and Sons, New York.

Pinarbasi, A. & Liakopoulos A. 1995 The effect of variable viscosity on the interfacial stability of two-layer Pouiseuille flow. *Physics of Fluids.* **7** (6), 1318-1324.

Schlichting, H. 1979 *Boundary Layer Theory*. McGraw-Hill, New York.

Shivamoggi, B. K. 1986 *Stability of Parallel Gas Flows*. John Wiley and Sons, New York.

Shoemaker, D. P. et. al. 1981 *Experiments in Physical Chemistry*. McGraw-Hill Book Company, New York.

Tatsumi, T. & Goth, K. 1959 The stability of free boundary layers between two uniform streams. *J. Fluid Mech.* **7**, 433-441.

Tatsumi, T. & Kakutani, T. 1958 The stability of a two-dimensional laminar jet. *Journal of Fluid Mechanics*. **4**, 261-275.

Thomas, L. H. 1953 The stability of plane poiseuille flow. *Physical Review*. **91** (4), 780-783.

Zebib, A. 1987 Removal of spurious modes encountered in solving stability problems by spectral methods. *J. Compt. Phys*. **70**, 521-525.

Appendix A

Using the Galerkin approach we approximate the highest derivatives of the function *f*, and the molar concentration by truncated sums of Chebyshev polynomials of the form

$$f_1'''(z_1) = \sum_{i=0}^{N} a_i T_i(z_1) \tag{A1a}$$

$$f_2'''(z_2) = \sum_{i=0}^{N} b_i T_i(z_2) \tag{A1b}$$

$$c_1''(z_1) = \sum_{i=0}^{N} c_i T_i(z_1) \tag{A1c}$$

$$c_2''(z_2) = \sum_{i=0}^{N} d_i T_i(z_2) \tag{A1d}$$

where N is the number of Chebyshev polynomials. The lower order terms are found by integrating the above equations, which yields the following.

$$f_1''(z_1) = \sum_{i=0}^{N}\sum_{j=0}^{N+1} a_i g_{ji}^{(2)} T_j(z_1) + A_1 \tag{A2a}$$

$$f_2''(z_2) = \sum_{i=0}^{N}\sum_{j=0}^{N+1} b_i g_{ji}^{(2)} T_j(z_2) + B_1 \tag{A2b}$$

$$f_1'(z_1) = \sum_{i=0}^{N}\sum_{j=0}^{N+2} a_i g_{ji}^{(1)} T_j(z_1) + A_1 z_1 + A_2 \tag{A2c}$$

$$f_2'(z_2) = \sum_{i=0}^{N}\sum_{j=0}^{N+2} b_i g_{ji}^{(1)} T_j(z_2) + B_1 z_2 + B_2 \tag{A2d}$$

$$f_1(z_1) = \sum_{i=0}^{N}\sum_{j=0}^{N+3} a_i g_{ji}^{(0)} T_j(z_1) + A_1 \frac{z_1^2}{2} + A_2 z_1 + A_3 \tag{A2e}$$

$$f_2(z_2) = \sum_{i=0}^{N}\sum_{j=0}^{N+3} b_i g_{ji}^{(0)} T_j(z_2) + B_1 \frac{z_2^2}{2} + B_2 z_2 + B_3 \tag{A2f}$$

$$c_1'(z_1) = \sum_{i=0}^{N} \sum_{j=0}^{N+1} c_i g_{ji}^{(1)} T_j(z_1) + C_1 \tag{A2g}$$

$$c_2'(z_2) = \sum_{i=0}^{N} \sum_{j=0}^{N+1} d_i g_{ji}^{(1)} T_j(z_2) + D_1 \tag{A2h}$$

$$c_1(z_1) = \sum_{i=0}^{N} \sum_{j=0}^{N+2} c_i g_{ji}^{(0)} T_j(z_1) + C_1 z_1 + C_2 \tag{A2i}$$

$$c_2(z_2) = \sum_{i=0}^{N} \sum_{j=0}^{N+2} d_i g_{ji}^{(0)} T_j(z_2) + D_1 z_2 + D_2 \tag{A2j}$$

The functions $g^{(\sigma)}{}_{ji}$, (σ = 0,1,2) are obtained by applying the following properties of Chebyshev polynomials.

$$2T_n(z) = \frac{\alpha_n}{n+1} \frac{d\,T_{n+1}(z)}{dz} - \frac{\lambda_{n-2}}{n-1} \frac{d\,T_{n-1}(z)}{dz} \tag{A3a}$$

and

$$2zT_n(z) = \alpha_n T_{n+1}(z) - \lambda_{n-1} T_{n-1}(z) \tag{A3b}$$

where $\alpha_n = \lambda_n = 0$ if $n < 0$, $\alpha_0 = 2$, $\lambda_0 = 1$, and $\alpha_n = \lambda_n = 1$ if n > 0, which are given by Zebib (1987). The constants A_1, A_2, A_3, B_1, B_2, B_3, C_1, C_2, D_1, and D_2 are determined by using the boundary conditions. The functions and derivatives of f_1, f_2, c_1, and c_2 are

$$f_1''' = \sum_{i=0}^{N} a_i T_i \tag{A4a}$$

$$f_1'' = \sum_{i=0}^{N} \sum_{j=0}^{N+1} a_i h_{1aji}^{(2)} T_j + \sum_{i=0}^{N} \sum_{j=0}^{N+1} b_i h_{1bji}^{(2)} T_j + T_0 k_1 \tag{A4b}$$

$$f_1' = \sum_{i=0}^{N} \sum_{j=0}^{N+2} a_i h_{1aji}^{(1)} T_j + \sum_{i=0}^{N} \sum_{j=0}^{N+2} b_i h_{1bji}^{(1)} T_j + T_1 k_1 + T_0 k_2 \tag{A4c}$$

$$f_1 = \sum_{i=0}^{N}\sum_{j=0}^{N+3} a_i h_{1aji}^{(0)} T_j + \sum_{i=0}^{N}\sum_{j=0}^{N+3} b_i h_{1bji}^{(0)} T_j + z_1^2 k_1 + T_1 k_2 + T_0 k_3 \tag{A4d}$$

$$c_1^{''} = \sum_{i=0}^{N} c_i T_i \tag{A4e}$$

$$c_1^{'} = \sum_{i=0}^{N}\sum_{j=0}^{N+1} c_i h_{1cji}^{(1)} T_j + \sum_{i=0}^{N}\sum_{j=0}^{N+1} d_i h_{1dji}^{(1)} T_j + T_0 k_4 \tag{A4f}$$

$$c_1 = \sum_{i=0}^{N}\sum_{j=0}^{N+2} c_i h_{1cji}^{(0)} T_j + \sum_{i=0}^{N}\sum_{j=0}^{N+2} d_i h_{1dji}^{(0)} T_j + T_1 k_4 + T_0 k_5 \tag{A4g}$$

$$f_2^{''''} = \sum_{i=0}^{N} b_i T_i \tag{A4h}$$

$$f_2^{''} = \sum_{i=0}^{N}\sum_{j=0}^{N+1} b_i h_{2bji}^{(2)} T_j + \sum_{i=0}^{N}\sum_{j=0}^{N+1} a_i h_{2aji}^{(2)} T_j + T_0 k_6 \tag{A4i}$$

$$f_2^{'} = \sum_{i=0}^{N}\sum_{j=0}^{N+2} b_i h_{2bji}^{(1)} T_j + \sum_{i=0}^{N}\sum_{j=0}^{N+2} a_i h_{2aji}^{(1)} T_j + T_1 k_6 + T_0 k_7 \tag{A4j}$$

$$f_2 = \sum_{i=0}^{N}\sum_{j=0}^{N+3} b_i h_{2bji}^{(0)} T_j + \sum_{i=0}^{N}\sum_{j=0}^{N+3} a_i h_{2aji}^{(0)} T_j + z_1^2 k_6 + T_1 k_7 + T_0 k_9 \tag{A4k}$$

$$c_2^{''}(z_2) = \sum_{i=0}^{N} d_i T_i(z_2) \tag{A4l}$$

$$c_2^{'} = \sum_{i=0}^{N}\sum_{j=0}^{N+1} d_i h_{2dji}^{(1)} T_j + \sum_{i=0}^{N}\sum_{j=0}^{N+1} c_i h_{2cji}^{(1)} T_j + T_0 k_9 \tag{A4m}$$

$$c_2 = \sum_{i=0}^{N}\sum_{j=0}^{N+2} d_i h_{2dji}^{(0)} T_j + \sum_{i=0}^{N}\sum_{j=0}^{N+2} c_i h_{2cji}^{(0)} T_j + T_1 k_9 + T_0 k_{10} \tag{A4n}$$

where the constants A_1, A_2, A_3, B_1, B_2, B_3, C_1, C_2, D_1, and D_2; and the functions $g^{(\sigma)}{}_{ji}$, (σ = 0,1,2) are combined into the functions $h^{(\sigma)}{}_{ji}$ (σ = 0, 1, 2). It should be noted that due to the boundary conditions at the interface (z = -1) there exists cross terms in the lower order

derivatives due to interdependence of the integration constants. The constants k_1 through k_{10} represent the nonhomogeneous parts of the integration constants. The Chebyshev expansions are then substituted into the base state governing equations. The inner products are formed with

$$\sum_{j=0}^{N+3} h_{kaji}^{(0)} T_j, \quad \sum_{j=0}^{N+3} h_{kbji}^{(0)} T_j, \quad \sum_{j=0}^{N+2} h_{kcji}^{(0)} T_j, \quad \text{and} \quad \sum_{j=0}^{N+2} h_{kdji}^{(0)} T_j \tag{A5}$$

The above procedure reduces the solutions of ordinary differential equations to a set of nonlinear algebraic equations. Standard Newton-Raphson iteration is used to reduce these equations to the set of linear equations,

$$\mathbf{A}\mathbf{x} + \mathbf{b} = 0 \tag{A6}$$

which is solved using an IMSL sub-routine.

Appendix B

Using the Galerkin approach we approximate the highest derivatives of the amplitude functions ϕ, and κ, by truncated sums of Chebyshev polynomials of the form

$$\phi_1'''' = \sum_{i=0}^{N} a_i T_i \tag{B1a}$$

$$\kappa_1'' = \sum_{i=0}^{N} c_i T_i \tag{B1b}$$

$$\phi_2'''' = \sum_{i=0}^{N} b_i T_i \tag{B1c}$$

$$\kappa_2'' = \sum_{i=0}^{N} d_i T_i \tag{B1d}$$

where N is the number of Chebyshev polynomials. The lower order terms are found by integrating the above equations, which yields the following.

$$\phi_1''' = \sum_{i=0}^{N}\sum_{j=0}^{N+1} a_i g_{ji}^{(3)} T_j + A_1 \tag{B2a}$$

$$\phi_1'' = \sum_{i=0}^{N}\sum_{j=0}^{N+2} a_i g_{ji}^{(2)} T_j + A_1\xi_1 + A_2 \tag{B2b}$$

$$\phi_1' = \sum_{i=0}^{N}\sum_{j=0}^{N+3} a_i g_{ji}^{(1)} T_j + A_1\frac{\xi_1^2}{2} + A_2\xi_1 + A_3 \tag{B2c}$$

$$\phi_1 = \sum_{i=0}^{N}\sum_{j=0}^{N+4} a_i g_{ji}^{(0)} T_j + A_1\frac{\xi_1^3}{6} + A_2\frac{\xi_1^2}{2} + A_3\xi_1 + A_4 \tag{B2d}$$

$$\kappa_1' = \sum_{i=0}^{N}\sum_{j=0}^{N+1} c_i g_{ji}^{(1)} T_j + C_1 \tag{B2e}$$

$$\kappa_1 = \sum_{i=0}^{N}\sum_{j=0}^{N+2} c_i g_{ji}^{(0)} T_j + C_1\xi_1 + C_2 \tag{B2f}$$

$$\phi_2''' = \sum_{i=0}^{N}\sum_{j=0}^{N+1} b_i g_{ji}^{(3)} T_j + B_1 \tag{B2g}$$

$$\phi_2'' = \sum_{i=0}^{N}\sum_{j=0}^{N+2} b_i g_{ji}^{(2)} T_j + B_1\xi_2 + B_2 \tag{B2h}$$

$$\phi_2' = \sum_{i=0}^{N}\sum_{j=0}^{N+3} b_i g_{ji}^{(1)} T_j + B_1\frac{\xi_2^2}{2} + B_2\xi_2 + B_3 \tag{B2i}$$

$$\phi_2 = \sum_{i=0}^{N}\sum_{j=0}^{N+4} b_i g_{ji}^{(0)} T_j + B_1\frac{\xi_2^3}{6} + B_2\frac{\xi_2^2}{2} + B_3\xi_2 + B_4 \tag{B2j}$$

$$\kappa_2' = \sum_{i=0}^{N}\sum_{j=0}^{N+1} d_i g_{ji}^{(1)} T_j + D_1 \tag{B2k}$$

$$\kappa_2 = \sum_{i=0}^{N}\sum_{j=0}^{N+2} d_i g_{ji}^{(0)} T_j + D_1\xi_2 + D_2 \tag{B2l}$$

The functions $g^{(\sigma)}{}_{ji}$, (σ = 0, 1, 2, 3) are obtained by applying the following properties of Chebyshev polynomials.

$$2T_n(z) = \frac{\alpha_n}{n+1}\frac{dT_{n+1}(z)}{dz} - \frac{\lambda_{n-2}}{n-1}\frac{dT_{n-1}(z)}{dz} \tag{B3a}$$

and

$$2zT_n(z) = \alpha_n T_{n+1}(z) - \lambda_{n-1}T_{n-1}(z) \tag{B3b}$$

where $\alpha_n = \lambda_n = 0$ if $n < 0$, $\alpha_0 = 2$, $\lambda_0 = 1$, and $\alpha_n = \lambda_n = 1$ if n > 0, which are given by Zebib (1987). The constants $A_1, A_2, A_3, A_4, B_1, B_2, B_3, B_4, C_1, C_2, D_1$, and D_2 are determined by using the boundary conditions. The functions and derivatives of ϕ_1, ϕ_2, κ_1, and κ_2 are

$$\phi_1'''' = \sum_{i=0}^{N} a_i T_i \tag{B4a}$$

$$\phi_1''' = \sum_{i=0}^{N}\sum_{j=0}^{N+1} a_i h_{1aji}^{(3)} T_j + \sum_{i=0}^{N}\sum_{j=0}^{N+1} b_i h_{1bji}^{(3)} T_j \tag{B4b}$$

$$\phi_1'' = \sum_{i=0}^{N}\sum_{j=0}^{N+2} a_i h_{1aji}^{(2)} T_j + \sum_{i=0}^{N}\sum_{j=0}^{N+2} b_i h_{1bji}^{(2)} T_j \tag{B4c}$$

$$\phi_1' = \sum_{i=0}^{N}\sum_{j=0}^{N+3} a_i h_{1aji}^{(1)} T_j + \sum_{i=0}^{N}\sum_{j=0}^{N+3} b_i h_{1bji}^{(1)} T_j \tag{B4d}$$

$$\phi_1 = \sum_{i=0}^{N}\sum_{j=0}^{N+4} a_i h_{1aji}^{(0)} T_j + \sum_{i=0}^{N}\sum_{j=0}^{N+4} b_i h_{1bji}^{(0)} T_j \tag{B4e}$$

$$\kappa_1'' = \sum_{i=0}^{N} c_i T_i \tag{B4f}$$

$$\kappa_1' = \sum_{i=0}^{N}\sum_{j=0}^{N+1} c_i h_{1cji}^{(1)} T_j + \sum_{i=0}^{N}\sum_{j=0}^{N+1} d_i h_{1dji}^{(1)} T_j \tag{B4g}$$

$$\kappa_1 = \sum_{i=0}^{N}\sum_{j=0}^{N+2} c_i h_{1cji}^{(0)} T_j + \sum_{i=0}^{N}\sum_{j=0}^{N+2} d_i h_{1dji}^{(0)} T_j \tag{B4h}$$

$$\phi_2'''' = \sum_{i=0}^{N} b_i T_i \tag{B4i}$$

$$\phi_2''' = \sum_{i=0}^{N}\sum_{j=0}^{N+1} b_i h_{2bji}^{(3)} T_j + \sum_{i=0}^{N}\sum_{j=0}^{N+1} a_i h_{2aji}^{(3)} T_j \tag{B4j}$$

$$\phi_2'' = \sum_{i=0}^{N}\sum_{j=0}^{N+2} b_i h_{2bji}^{(2)} T_j + \sum_{i=0}^{N}\sum_{j=0}^{N+2} a_i h_{2aji}^{(2)} T_j \tag{B4k}$$

$$\phi_2' = \sum_{i=0}^{N}\sum_{j=0}^{N+3} b_i h_{2bji}^{(1)} T_j + \sum_{i=0}^{N}\sum_{j=0}^{N+3} a_i h_{2aji}^{(1)} T_j \tag{B4l}$$

$$\phi_2 = \sum_{i=0}^{N}\sum_{j=0}^{N+4} b_i h_{2bji}^{(0)} T_j + \sum_{i=0}^{N}\sum_{j=0}^{N+4} a_i h_{2aji}^{(0)} T_j \tag{B4m}$$

$$\kappa_2'' = \sum_{i=0}^{N} d_i T_i \tag{B4n}$$

$$\kappa_2' = \sum_{i=0}^{N}\sum_{j=0}^{N+1} d_i h^{(1)}_{2dji} T_j + \sum_{i=0}^{N}\sum_{j=0}^{N+1} c_i h^{(1)}_{2cji} T_j \tag{B4o}$$

$$\kappa_2 = \sum_{i=0}^{N}\sum_{j=0}^{N+2} d_i h^{(0)}_{2dji} T_j + \sum_{i=0}^{N}\sum_{j=0}^{N+2} c_i h^{(0)}_{2cji} T_j \tag{B4p}$$

where the constants A_1, A_2, A_3, B_1, B_2, B_3, C_1, C_2, D_1, and D_2; and the functions $g^{(\sigma)}{}_{ji}$, (σ = 0, 1, 2, 3) are combined into the functions $h^{(\beta)}{}_{ji}$ (β = 0, 1, 2, 3). Again, it should be noted that due to the boundary conditions at the interface (z = -1) there exists cross terms in the lower order derivatives due to interdependence of the integration constants. The Chebyshev expansions are then substituted into the disturbance equations (2.31). The inner products are formed with

$$\sum_{j=0}^{N+4} h^{(0)}_{kaji} T_j, \quad \sum_{j=0}^{N+4} h^{(0)}_{kbji} T_j, \quad \sum_{j=0}^{N+2} h^{(0)}_{kcji} T_j, \quad \text{and} \quad \sum_{j=0}^{N+2} h^{(0)}_{kdji} T_j \tag{B5}$$

The above procedure reduces the solutions of ordinary differential equations to the set of nonlinear algebraic equations. Standard Newton-Raphson iteration is used to reduce these equations to the set of linear equations,

$$\mathbf{A}\mathbf{s} + \beta \mathbf{B}\mathbf{s} = 0 \tag{B6}$$

which is solved using an IMSL sub-routine.

Vita

Louis Cumbo was born in Rochester, New York, on January 5, 1971. He attended Gates-Chili High School and entered Syracuse University in 1989. In May, 1993, he received a Bachelor of Science in Aerospace Engineering. In August, 1993, he entered the Masters degree program in the Department of Mechanical Engineering at Lehigh University.

END

OF

TITLE